A Repairable System Subjected to Hierarchical Competing Risks: Modeling and Applications

FRANCISCO LOUZADA[1], JOSÉ A. CUMINATO[1], OSCAR M.H. RODRIGUEZ[2], VERA L.D. TOMAZELLA[3], PAULO H. FERREIRA[1], PEDRO L. RAMOS[1], SEYED R.A. NIAKI[1], OILSON A. GONZATTO JUNIOR[1], IVAN C. PERISSINI[2], LUIS F.A. ALEGRÍA [2], DANILO COLOMBO[4], DAVID E.A. MARTINS[4], HUGO F.L. SANTOS[4] ,

[1]Institute of Mathematical and Computer Sciences (ICMC), University of São Paulo, São Carlos, SP, Brazil
[2]São Carlos School of Engineering (EESC), University of São Paulo, São Carlos, SP, Brazil
[3]Department of Statistics (DEs), Federal University of São Carlos, São Carlos, SP, Brazil
[4]Leopoldo Américo Miguez de Mello Research and Development Center (CENPES - Petrobras), Rio de Janeiro, RJ, Brazil

Corresponding author: Pedro L. Ramos (e-mail: pedrolramos@usp.br).

The research was supported by the Agência Nacional do Petróleo (ANP) and Petrobras, Brazil.

ABSTRACT In this paper, we propose modeling for a single repairable system with a hierarchical structure under the assumption that the failures follow a nonhomogeneous Poisson process (which corresponds to minimal repair action) with a power-law intensity function. The properties of the new model are discussed in detail. The parameter estimators are obtained using the maximum likelihood method. A corrective approach is used to remove bias with order $O(n^{-1})$, and the respective exact confidence intervals are proposed. A simulation study is conducted to show that our estimators are bias-free. The proposed modeling is illustrated via a toy example on a butterfly valve system, an example of an early-stage real project related to the traction system of an in-pipe robot, and also a real example on a blowout preventer system.

INDEX TERMS
Bias correction, Competing risks, Hierarchical systems, Maximum likelihood estimation, Parametric statistics, Power-law process, Reliability engineering

I. INTRODUCTION

THE presence of repeated recurrences of an event of interest often arises in areas such as manufacturing, software development, medical applications, social sciences, and risk analysis, among others. In reliability engineering, when a complex system such as supercomputers, airplanes or cars is included in a study, several unexpected failures may be exposed by different defects or weaknesses in the products' design, manufacturing, operation, maintenance, and management [1]. Models with this feature are traditionally referred to as competing risks, or equivalently, a system with p components connected in series. A single component failure results in total system failure.

Recently, the availability evaluation of repairable systems with multiple failure modes is at the center of attention due to the broad application in engineering. According to the competing risks framework, a series system fails by the earliest occurrence of failure modes. Therefore, in this paper, we utilized a model for components, whose failures happen due to one of the series competing failure mechanisms, whereby each of them acts related to the system independently.

A system can be broken down into several sub-systems, and sub-sub-systems compose the sub-systems in a hierarchical form until the elements cannot or are not worthy of being divided. The system's hierarchies can help engineers to better understand the relationships between components and their importance and functions. They can further help engineers to determine the role and acceptable damaging degree of each part of the structure and their influences on the whole system under various external forces and effects [2].

Thus, structuring a problem according to a hierarchy can help to increase accuracy and facilitate useful analysis of failure factors. Note that the event of interest at the system level is expected to happen at its earliest occurrence. Therefore, a system can be anticipated to follow a competing risks model. As an example given by Liu et al. [3], mechanical devices

(e.g., gear pair and crank train) are always under multiple failure modes (including fracture, corrosion and wear), which compete with each other so that when one kind of failure happens, the device is invalid and other failure modes have no chance to occur anymore.

The components under consideration are repaired upon failure but are also preventively maintained. Thus, the excellent books by Crowder [4] and Pintilie [5], among others, motivate the need for accounting for competing risks in reliability and survival applications using several examples in industrial statistics and health sciences. More recently, Langseth and Lindqvist [6] recorded cumulative service times of a component spanning over 1,600 time units, then marking each failure with its specific causing mode. In this case, the causes were categorized into two broad groups, each with several specified sub-causes. Tuli et al. [7] analyzed repeated shunt failures in infants diagnosed with hydrocephalus, where the failures are known to occur due to a variety of causes.

In this paper, the focus is placed on failure data from repairable systems. Thus, solid modeling and analysis of this data provide equipment operators for better maintenance activities. In the repairable system literature, it is often assumed that failures occur following a nonhomogeneous Poisson process (NHPP) with power-law intensity. The resulting process is usually referred to as the power-law process (PLP). Proposed by Crow [8], the PLP is convenient because it is easy to implement, flexible, and the parameters have valuable interpretation ([9], [10]). In the literature, the PLP has been widely used in modeling software reliability [11], reliability growth [12], repairable systems ([9], [13], [14]), etc. Appropriateness of the PLP for a particular dataset can be verified either by graphical methods, such as the Duane plots [15] and modified total time on test (TTT) plots [16], or by formal hypothesis tests ([17], [18]). Regarding classical inference for the PLP, see, e.g., Ascher and Feingold [13] or Ridgon and Basu [19]. Bayesian inference has been considered, among others, by Bar-Lev et al. [20] and Guida et al. [21]. Along these lines, Oliveira et al. [22] introduced an orthogonal parametrization of the PLP, which simplifies both the analysis and interpretation of the results. The most commonly used models for repairable systems assume either perfect repair (renewal process models) or minimal repair (NHPP models).

The main aim of this paper is to propose a hierarchical model for a repairable system subject to several failure modes (competing risks). Under minimal repair, it is assumed that each failure mode has a power-law intensity. Hence, we develop a new PLP model with a minimal repair under competing risks, which generalizes the model presented in Somboonsavatdee and Sen [23]. Furthermore, we discuss the inferential procedure for the parameters of the proposed model using the maximum likelihood estimators (MLEs), as well as the asymptotic confidence intervals based on the MLEs. Since the sample size is usually small, due to the problem of rare yet adverse failures in industrial scenarios (e.g., in aerospace, nuclear and petrochemical industries) that causes limited failure data availability, we may obtain biased estimators and unreliable asymptotic confidence intervals. To overcome this problem, we suggest a corrective approach to obtain unbiased estimators for the model parameters. Additionally, we discuss how to derive exact confidence intervals based on these unbiased estimators.

The paper is organized as follows. In Section II, we give some basic concepts about counting processes, repairable systems, and competing risks models. This section also presents the framework of recurrent competing risks for the minimal repair model. In Section III, we present a new statistical model to analyze single repairable systems with a hierarchical structure under the assumption that the repairs are minimal with a PLP intensity and also in the presence of competing risks. In Section IV, we discuss classical inference for the model parameters through the MLEs and asymptotic confidence intervals and also perform a simulation study to investigate their properties. In Section V, we develop improved estimators (bias-corrected MLEs), as well as exact confidence intervals for the model parameters, whose performances are again evaluated through a simulation study. In Section VI, we illustrate our proposed methodology using simulated reliability data of butterfly valves (Section VI-A), reliability data based on an in-pipe robot traction system design information (real project in its early stage) (Section VI-B), and real reliability data of blowout preventer systems (Section VI-C). Finally, in Section VII, we conclude the paper with some final remarks and suggestions for work.

II. LITERATURE REVIEW

In this section, we briefly discuss the literature related to the failure analysis of a single repairable system with the particular assumptions that the repairs are minimal with a PLP intensity, and subject to failure due to competing risks. We also consider an orthogonal reparametrization of the PLP model, which enables us to obtain a likelihood function whose parameters are independent with desirable properties.

A. NONHOMOGENEOUS POISSON PROCESS

Let us suppose a repairable system with a single cause of failure, where $N(t)$ denotes the number of failures before time t, and $N(a,b] = N(b) - N(a)$ denotes the number of failures in the time interval $(a,b]$. In turn, a NHPP with intensity function $\lambda(t)$, $t \geq 0$, is a counting process with independent increments, and we have

$$\lambda(t) = \lim_{\Delta t \to 0} \frac{P(N(t, t+\Delta t] \geq 1)}{\Delta t}.$$

The mean of the Poisson distribution for the random variable $N(t)$, at time t, is denoted as $\Lambda(t) = \int_0^t \lambda(s)ds$. A flexible parametric form for the intensity function is given by

$$\lambda(t) = \left(\frac{\beta}{\mu}\right)\left(\frac{t}{\mu}\right)^{\beta-1}, \qquad (1)$$

where $\mu, \beta > 0$. In this case, the NHPP represents a PLP with mean function

$$\Lambda(t) = \mathbb{E}[N(t)] = \int_0^t \lambda(s)ds = \left(\frac{t}{\mu}\right)^{\beta}.$$

The scale parameter μ is the time for which we expect to observe only one event. In turn, β is the elasticity of the mean number of events with respect to time [22].

Notice also that (1) is an increasing (decreasing) function in t for $\beta > 1$ ($\beta < 1$). In this case, the PLP can reflect the possibility of improvement or deterioration of the system over time. It is worth noting that, when $\beta = 1$, the intensity function (1) is constant, and the PLP reduces to a homogeneous Poisson process.

B. MINIMAL REPAIR MODEL

A major challenge when modeling repairable system data is how to consider the effect of a repair action taken immediately after a failure has occurred. It is usually supposed, for the sake of simplicity, that the repair actions are instantaneous. However, it is not suitable for many real systems. Therefore, the most investigated assumptions are either minimal or perfect repair at failures. In the former, it is assumed that the repair action after a failure restores the system (i.e., the intensity) to the same state as it was before the failure, e.g., by replacing a failed minor component (flat tire) of a large composite system (car); while in the latter, the repair action leaves the system as if it was new, e.g., via replacement of a failed system (an engine with a broken connecting rod) by a brand new one [24]. According to the engineering literature, these repair or maintenance actions are often called ABAO ("as bad as old") and AGAN ("as good as new"), respectively ([25], [26], [27], [28], [29]). However, more complex models suppose that the repair effect lies between ABAO and AGAN (i.e., the failure intensity is reduced to a level between ABAO and AGAN). These models are known as imperfect repair models, but they are not considered here (see, e.g., [30]).

In fact, the repairable system model for the failure data will be implemented according to NHPP under the assumption of minimal repair. Furthermore, based on the time truncation design, the likelihood and corresponding log-likelihood function for a collection of failure data up to time T, are expressed as

$$L(\beta, \mu \mid n, \boldsymbol{t}) = \frac{\beta^n}{\mu^{n\beta}} \left(\prod_{i=1}^{n} t_i\right)^{\beta-1} \exp\left\{-\left(\frac{T}{\mu}\right)^{\beta}\right\}$$

and

$$\begin{aligned}\ell(\beta, \mu \mid n, \boldsymbol{t}) =& n\log(\beta) + (\beta-1)\sum_{i=1}^{n}\log(t_i) \\ &- \left(\frac{T}{\mu}\right)^{\beta} - n\beta\log(\mu),\end{aligned}$$

respectively, where we assume that for $n \geq 1$, failures are observed at times $t_1 < t_2 < \cdots < t_n < T$ (see, e.g., [19]). The MLEs of β and μ, which are both biased, can be written as

$$\hat{\beta} = \frac{n}{\sum_{i=1}^{n}\log\left(\frac{T}{t_i}\right)} \quad \text{and} \quad \hat{\mu} = \frac{T}{n^{1/\hat{\beta}}}. \tag{2}$$

Since the MLEs (2) suffer from bias, and inadequate confidence intervals for small samples, several studies have been performed to overcome these drawbacks. Some further discussions are given in Section V.

There is always a concern about how to determine the confidence intervals under the classical inference. For the sake of illustration, Rigdon and Basu [19] present the confidence interval for the scale parameter. The results showed that such an interval has no simple interpretation. Moreover, the authors found that the usual methodologies result in very long intervals. In turn, in some cases, the pivotal quantity, which is used to derive the aforementioned classical intervals, does not exist, or it is difficult to be obtained. Bain and Engelhardt [31] extensively investigated confidence intervals for the scale parameter. The outcome of their research has shown that due to the non-existence of the pivotal quantity in the setting of time truncated data, finding confidence intervals for the scale parameter becomes difficult. Despite the extensive efforts, in most cases, the approaches still have limitations. For instance, Gaudoin et al. [32] studied the interval estimation for the scale parameter according to the PLP model. They used the Fisher information matrix to derive asymptotic confidence intervals, while several constraints have been reported on their results. Wang et al. [33] considered a more sophisticated approach to obtain a generalized confidence interval for the scale parameter under some usual assumptions. Furthermore, Somboonsavatdee and Sen [23] have shown methods to obtain the frequentist confidence intervals for the scale parameter under competing risks.

Oliveira et al. [22] suggested reparametrizing the PLP intensity in terms of β and α, where

$$\alpha = \mathbb{E}[N(T)] = \left(\frac{T}{\mu}\right)^{\beta}.$$

In this case, the likelihood function is given by

$$\begin{aligned}L(\beta, \alpha \mid n, \boldsymbol{t}) &= c\beta^n e^{-n\beta/\hat{\beta}}\alpha^n e^{-\alpha} \\ &\propto \gamma\left(\beta \mid n+1, n/\hat{\beta}\right)\gamma\left(\alpha \mid n+1, 1\right),\end{aligned}$$

where $c = \prod_{i=1}^{n} t_i^{-1}$ and $\gamma(x \mid a, b) = b^a x^{a-1} e^{-bx}/\Gamma(a)$, for $x, a, b > 0$, is the probability density function of a gamma distribution with shape parameter a and scale parameter b. It is worth mentioning that β and α are orthogonal parameters, which play an important role for Bayesian inference (see, e.g., [34]).

C. COMPETING RISKS

In reliability theory, the most commonly used system configurations are series, parallel, and series-parallel. Particularly, components in a series system are connected so that the failure of one of all components results in the system failure. For

example, Figure 1 illustrates the fault tree analysis (FTA) of the system $1, \ldots, p$. A series system is known as a competing risks model because its failure can be classified as one of the p possible risks (or failure modes), which compete with each other to occur first and cause the system failure. Competing risks can provide a complete analysis of the probabilistic behavior of failures as many other methodologies presented in the literature. However, competing risks has an additional feature addressing not only failure times but also their causes through a pair of observations. Furthermore, the competing risks model involves the pair of observations (t, δ), where $t > 0$ denotes the failure time, while δ is the indicator of the component that failed.

In order to understand the competing risks framework for investigating repairable systems, a single system would be to consider successive failures at calendar time $0 < t_1 < \ldots < t_n < T$. Let us suppose that failures happen from an underlying competing risks structure, meaning that the system fails by the earliest occurrence of one of p exclusive failure modes. In this case, it is generally possible to observe the failure mode $\delta(t_i)$ at the failure time t_i. And for the system level, let us denote $\{N(t),\, t > 0\}$ the cumulative failure counter. In fact, if $N_j(t)$ represents the counting process corresponding to the j-th failure mode, it is easy to demonstrate that $N(t) = \sum_{j=1}^{p} N_j(t)$. The cause-specific intensity function of this process is

$$\lambda_j\left(t; \delta(t)\right) = \lim_{\Delta t \to 0} \frac{P\left(\delta(t) = j, N(t+\Delta t) - N(t) = 1 \mid N(s), 0 \leq s \leq t\right)}{\Delta t}, \tag{3}$$

for $j = 1, \ldots, p$.

According to equation (3), the time and the failure mode are stochastically independent if and only if $\lambda_1(t), \ldots, \lambda_p(t)$ are proportional to each other, giving a simple extension of a similar result from the competing risks literature in failure time modeling of non-repairable systems.

As pointed out by many works in the literature, complex repairable systems are mostly considered under the assumption of stochastic independence, which is based on the physically independent functioning of components (see, e.g., [35], [4], [36] and [37]). It is essential to mention that the current paper is also based on this common assumption of independent risks, or equivalently, independent failure modes.

D. MODELING MINIMAL REPAIR UNDER COMPETING RISKS

Let us assume that the system is observed up to time T, and that the adopted model is reparametrized in terms of β_j and

$$\alpha_j = \mathbb{E}[N_j(T)] = \left(\frac{T}{\mu_j}\right)^{\beta_j},$$

where $N_j(.)$ is the j-th cause-specific counting process, for $j = 1, \ldots, p$. This implies that β_j and α_j are orthogonal parameters.

A common strategy is to assume that the components of the repairable system under investigation can implement different operations, which are subject to different kinds of failure. Let us consider p failure modes, which at each failure are denoted by $\delta(t) = j$, for $j = 1, \ldots, p$ (in the sequel, we will suppress the explicit dependence of δ on failure time t for brevity). Thus, if n failures are observed in the time interval $(0, T]$, then we have the data $(t_1, \delta_1), \ldots, (t_n, \delta_n)$, where $0 < t_1 < \cdots < t_n < T$ are the system failure times, and the δ_i's indicate the j-th failure mode associated with the i-th failure time, for $i = 1, \ldots, n$.

Let us consider again the counting process $N_j(t)$ with behavior according to the cause-specific intensity function

$$\lambda_j(t; \delta) = \lim_{\Delta t \to 0} \frac{P(\delta = j, N(t, t+\Delta t] \geq 1)}{\Delta t}.$$

Consequently, $N(t) = \sum_{j=1}^{p} N_j(t)$, which is the global system failure counting process, can be seen as a superposition of NHPPs whose intensity function is given by

$$\lambda(t; \delta) = \sum_{j=1}^{p} \lambda_j(t; \delta).$$

The corresponding cause-specific and overall cumulative intensities are given, respectively, by

$$\Lambda_j(T) = \int_0^T \lambda_j(u; \delta)\, du \qquad \text{and} \qquad \Lambda(T) = \sum_{j=1}^{p} \Lambda_j(T).$$

Under the assumption that the failures from the j-th cause follow a NHPP with intensity function (1), we can write the cause-specific intensities as

$$\lambda_j(t; \delta) = \left(\frac{\beta_j}{\mu_j}\right)\left(\frac{t}{\mu_j}\right)^{\beta_j - 1}$$

and

$$\Lambda_j(T) = \left(\frac{T}{\mu_j}\right)^{\beta_j} = \mathbb{E}[N_j(T)],$$

for $j = 1, \ldots, p$.

III. HIERARCHICAL COMPETING RISKS MODEL

In this section, we propose to analyze failure data representing events from a single repairable system studied under the parametric framework of a PLP that is subject to hierarchical competing risks. It consists of a generalization of the work done by Somboonsavatdee and Sen [23] for the cases where there is the presence of secondary failure causes (subsystems or sub-trees' branches), as illustrated in Figure 1. The hierarchical competing risks problem/structure can also be represented by a block diagram showing a nested series system, where the sub-systems (and also the systems) are connected in such a way that the failure of a single subsystem (or component) results in the corresponding system failure and, consequently, in the whole system failure (see Figure 2).

The hierarchical competing risks model's data consist of 3-tuples (t, δ, ψ), where $t > 0$ denotes the failure time, δ is the indicator of the leading failure cause (system), and ψ is the indicator of the sub-cause (sub-system).

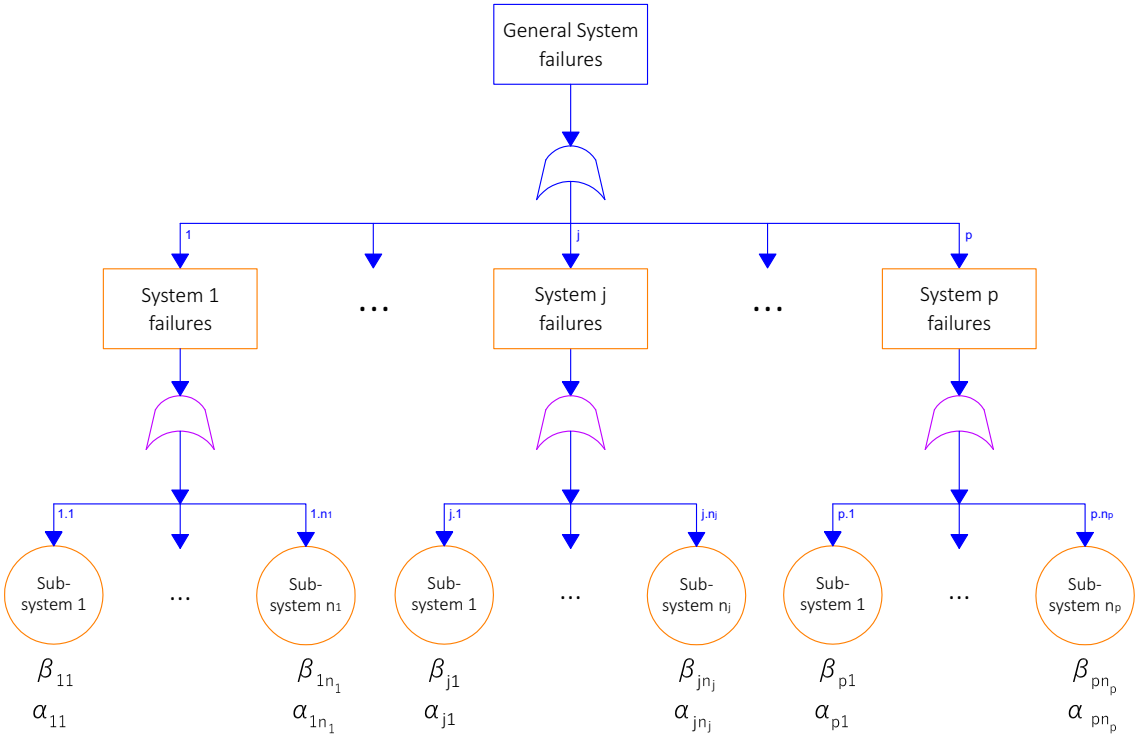

FIGURE 1: The general system structure (FTA) considering our proposed hierarchical competing risks model.

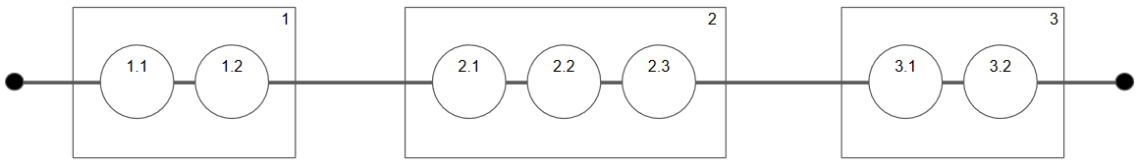

FIGURE 2: Block diagram for a nested series system with 2, 3 and 2 series sub-systems (or components) within series systems 1, 2 and 3, respectively.

Then, our proposed model for failure analysis can be formulated as follows. First, we assume that the failures from a sub-system k of a system j follow an NHPP with intensity function given by

$$\lambda_{jk}(t;\delta,\psi) = \left(\frac{\beta_{jk}}{\mu_{jk}}\right)\left(\frac{t}{\mu_{jk}}\right)^{\beta_{jk}-1}, \qquad (4)$$

for $j = 1,\ldots,p$, and $k = 1,\ldots,n_j$, with n_j being the number of sub-systems for the j-th system; $\mu_{jk} > 0$ and $\beta_{jk} > 0$ are, respectively, the scale and shape parameters.

It follows that

$$\lambda(t) = \sum_{j=1}^{p}\sum_{k=1}^{n_j}\lambda_{jk}(t;\delta,\psi) \qquad (5)$$

is the hazard function at time t. The sub-system-specific cumulative intensity is

$$\Lambda_{jk}(T) = \left(\frac{T}{\mu_{jk}}\right)^{\beta_{jk}}. \qquad (6)$$

Here, we assumed that the failure causes related to the sub-systems are independent, therefore we expect that the failures may occur at different times. Nevertheless, if the failure of two or more sub-systems happens occasionally at the same time, the sub-system-specific cumulative intensity for each sub-system can be calculated from (6), hence the intensity function (5) can be computed in the presence of multiple failures at the same time.

It is seen from (5) that $\Lambda(T) = \sum_{j=1}^{p}\sum_{k=1}^{n_j}\Lambda_{jk}(T)$ is the cumulative hazard function at time T. Thus, we have that the

reliability function is given by

$$R(T) = \exp\{-\Lambda(T)\} = \exp\left\{-\sum_{j=1}^{p}\sum_{k=1}^{n_j}\Lambda_{jk}(T)\right\}, \quad (7)$$

while the sub-system-specific reliability function is

$$R_{jk}(T) = \exp\{-\Lambda_{jk}(T)\}. \quad (8)$$

Then, similarly as in Section II-D, we consider that the sub-system's lifetime is observed up to time T and we reparametrize our model in terms of β_{jk} and

$$\alpha_{jk} = \mathbb{E}[N_{jk}(T)] = \left(\frac{T}{\mu_{jk}}\right)^{\beta_{jk}}, \quad (9)$$

where $N_{jk}(.)$ is the j-th system and k-th sub-system-specific counting process.

IV. INFERENCE

In this section, we describe classical inference for the model that we introduced in Section III. The MLEs and Fisher information matrix, which is used for estimating the asymptotic variances of the MLEs, are presented here.

Given the common (but sometimes unrealistic [1]) assumption that the failure modes act independently and are mutually exclusive, the classical inference for the proposed model is conducted using the likelihood function, or equivalently, the log-likelihood function, which are defined, respectively, as follows:

$$L(\boldsymbol{\theta} \mid \boldsymbol{t}, \boldsymbol{\delta}, \boldsymbol{\psi}) = \prod_{i=1}^{n}\prod_{j=1}^{p}\prod_{k=1}^{n_j}[\lambda_{jk}(t_i;\delta_i,\psi_i)]^{\mathbb{I}(\delta_i=j,\psi_i=k)} \exp\left\{-\sum_{j=1}^{p}\sum_{k=1}^{n_j}\Lambda_{jk}(T)\right\} \quad (10)$$

and

$$\ell(\boldsymbol{\theta} \mid \boldsymbol{t}, \boldsymbol{\delta}, \boldsymbol{\psi}) = \sum_{i=1}^{n}\sum_{j=1}^{p}\sum_{k=1}^{n_j}\mathbb{I}(\delta_i = j, \psi_i = k)\times \log\left(\lambda_{jk}(t_i;\delta_i,\psi_i)\right) - \sum_{j=1}^{p}\sum_{k=1}^{n_j}\Lambda_{jk}(T), \quad (11)$$

where $\boldsymbol{\theta} = \left(\beta_{11},\ldots,\beta_{pn_p},\alpha_{11},\ldots,\alpha_{pn_p}\right)$ denotes the general parameter vector; $\lambda_{jk}(t_i;\delta_i,\psi_i)$ and $\Lambda_{jk}(T)$ are given by (4) and (6), respectively; and $\mathbb{I}(\delta_i = j, \psi_i = k)$ is an indicator function. Before going further, it is important to mention again that our model is a generalization of the work by Somboonsavatdee and Sen [23], which estimates the PLP in the presence of competing risks. However, our model has an additional hierarchical structure, and thus the proposed estimators require a comprehensive investigation to be performed.

The MLEs can be obtained by maximizing the log-likelihood function (11). After some algebraic manipulation, such estimators can be written as

$$\hat{\beta}_{jk} = \frac{n_{jk}}{\sum_{i=1}^{n}\log\left(\frac{T}{t_i}\right)\mathbb{I}(\delta_i = j, \psi_i = k)} \quad (12)$$

and

$$\hat{\alpha}_{jk} = n_{jk}, \quad (13)$$

where n_{jk} denotes the total number of failures due to the subcause k of the major cause j.

Since from (9), $\mathbb{E}[N_{jk}(T)] = \alpha_{jk}$, we have that the Fisher information matrix can be expressed as

$$I(\boldsymbol{\theta}) = \text{Diag}(\alpha_{11}\beta_{11}^{-2},\ldots,\alpha_{1n_1}\beta_{1n_1}^{-2},\ldots,\alpha_{p1}\beta_{p1}^{-2},\ldots, \alpha_{pn_p}\beta_{pn_p}^{-2},\alpha_{11}^{-1}\ldots,\alpha_{1n_1}^{-1},\ldots,\alpha_{p1}^{-1}\ldots,\alpha_{pn_p}^{-1}), \quad (14)$$

where $\text{Diag}(\cdot)$ is a $\kappa \times \kappa$ diagonal matrix, with $\kappa = 2\sum_{j=1}^{p} j \times n_j$. The MLEs have a closed-form expression and unique solution, consequently from the Central Limit Theorem, they are asymptotically normally distributed with a multivariate normal distribution, which can be given by

$$\hat{\boldsymbol{\theta}} \sim N_{\kappa}\left(\boldsymbol{\theta}, I^{-1}(\boldsymbol{\theta})\right) \quad \text{as} \quad n_{jk} \to \infty. \quad (15)$$

A. SIMULATION STUDY

We conducted a simulation study to investigate the consistency and efficiency of the MLEs presented in equations (12) and (13). To that end, we used two criteria: the bias and mean square error (MSE), which are given, respectively, by $\text{Bias}\left(\hat{\theta}_w\right) = (1/M)\sum_{m=1}^{M}\left(\hat{\theta}_w^{(m)} - \theta_w\right)$ and $\text{MSE}\left(\hat{\theta}_w\right) = (1/M)\sum_{m=1}^{M}\left(\hat{\theta}_w^{(m)} - \theta_w\right)^2$, for $w = 1,\ldots,\kappa$, where $M = 50,000$ is the number of Monte Carlo replications and $\boldsymbol{\theta} = (\theta_1,\ldots,\theta_\kappa) = \left(\beta_{11},\ldots,\beta_{pn_p},\alpha_{11},\ldots,\alpha_{pn_p}\right)$ represents the parameter vector. Moreover, $\hat{\theta}_w^{(m)}$ denotes the MLE of θ_w obtained from sample m, for $m = 1,\ldots,M$.

By this approach, it is expected that good estimators have both bias and MSE close to zero. In turn, reasonable confidence intervals, which are produced here using the asymptotic normality of the MLEs (as given in equation (15)), are expected to be short with coverage probabilities close to the nominal value of 95%. In this work, all computations and simulations were performed using the R software (R Core Team, 2019).

In what follows, we present the results for a single system subject to 2 failure causes each with 3 sub-causes (Scenarios 1, 2 and 3), or 3 failure causes with 2, 3 and 2 sub-causes, respectively (Scenarios 4, 5 and 6), both under the assumption that the component system is observed in the fixed time interval $(0, T]$, where $T = 20$. Hence, four different scenarios (described below), with different parameter values in order to yield distinct sample sizes, are examined.

[1] As pointed out by Meeker and Escobar [38], it is possible that the failure of one component may either degrade or improve the reliability of other components, thus leading to either a positive or negative correlation between failure times in different system's components. Moreover, when this dependence exists, it is usually positive, since short (long) failure times of one mode tend to go with short (long) failure times of another.

- **Scenario 1:** $\beta_{11} = 0.8, \alpha_{11} = 3.30, \beta_{12} = 0.5, \alpha_{12} = 2.23, \beta_{13} = 1.0, \alpha_{13} = 7.0, \beta_{21} = 1.0, \alpha_{21} = 4.0, \beta_{22} = 1.0, \alpha_{22} = 2.0, \beta_{23} = 1.1, \alpha_{23} = 2.0$;
- **Scenario 2:** $\beta_{11} = 1.2, \alpha_{11} = 14.56, \beta_{12} = 0.9, \alpha_{12} = 10.37, \beta_{13} = 1.0, \alpha_{13} = 12.0, \beta_{21} = 1.0, \alpha_{21} = 4.0, \beta_{22} = 2.0, \alpha_{22} = 20.0, \beta_{23} = 1.2, \alpha_{23} = 10.92$;
- **Scenario 3:** $\beta_{11} = 1.2, \alpha_{11} = 10.92, \beta_{12} = 1.1, \alpha_{12} = 13.49, \beta_{13} = 1.2, \alpha_{13} = 12.74, \beta_{21} = 1.5, \alpha_{21} = 17.89, \beta_{22} = 1.8, \alpha_{22} = 21.97, \beta_{23} = 1.6, \alpha_{23} = 12.07$;
- **Scenario 4:** $\beta_{11} = 2.0, \alpha_{11} = 8.0, \beta_{12} = 0.4, \alpha_{12} = 4.97, \beta_{21} = 0.6, \alpha_{21} = 12.07, \beta_{22} = 0.7, \alpha_{22} = 12.21, \beta_{23} = 1.5, \alpha_{23} = 8.94, \beta_{31} = 0.4, \alpha_{31} = 9.94, \beta_{32} = 0.8, \alpha_{32} = 7.69$;
- **Scenario 5:** $\beta_{11} = 0.8, \alpha_{11} = 4.39, \beta_{12} = 0.8, \alpha_{12} = 8.24, \beta_{21} = 0.6, \alpha_{21} = 9.05, \beta_{22} = 0.3, \alpha_{22} = 4.67, \beta_{23} = 1.1, \alpha_{23} = 8.10, \beta_{31} = 0.5, \alpha_{31} = 8.94, \beta_{32} = 1.3, \alpha_{32} = 7.37$;
- **Scenario 6:** $\beta_{11} = 2.0, \alpha_{11} = 8.00, \beta_{12} = 1.1, \alpha_{12} = 40.48, \beta_{21} = 1.2, \alpha_{21} = 72.82, \beta_{22} = 1.1, \alpha_{22} = 40.48, \beta_{23} = 1.5, \alpha_{23} = 8.94, \beta_{31} = 1.1, \alpha_{31} = 80.96, \beta_{32} = 1.2, \alpha_{32} = 25.49$.

Due to space constraints, the results are reported only for these six scenarios. However, similar findings are obtained for other parameter choices.

By considering the well-known results regarding NHPPs [19], and also from the assumption that the failure modes are independent, we can generate the failure times, for each Monte Carlo replication, according to the following steps.

1. For the k-th sub-system of the j-th system, $j = 1, \ldots, p$, $k = 1, \ldots, n_j$, generate a random number $n_{jk} \sim \text{Poisson}\,(\Lambda_{jk}(T))$;
2. For the k-th sub-system of the j-th system, $j = 1, \ldots, p$, $k = 1, \ldots, n_j$, let the failure times be $t_{1,j,k}, \ldots, t_{n_{jk},j,k}$, where $t_{i,j,k} = T\,U_{i,j,k}^{1/\beta_{jk}}$ and $U_{1,j,k}, \ldots, U_{n_{jk},j,k}$ are the order statistics of a random sample of size n_{jk} from a Uniform$(0, 1)$ distribution;
3. Finally, in order to obtain the data in the form (t_i, δ_i, ψ_i), let the t_i's be the set of ordered failure times and make δ_i equal to j and ψ_i equal to k according to the corresponding failure mode and subcause, respectively (i.e., set $\delta_i = 1$ and $\psi_i = 1$ if $t_i = t_{h,1,1}$ for some h, or $\delta_i = j$ and $\psi_i = k$ depending on the failure mode and subcause).

As shown in Tables 1 and 2, the bias of the MLEs varies depending on the α_{jk} parameter values, i.e., the mean number of failures. If the values of α_{jk} are small, the bias of $\hat{\beta}_{jk}$ is considerably higher than expected, as well as the MSEs. This result is due to the systematic bias that the MLE of β_{jk} possesses. On the other hand, the maximum likelihood estimates of the α_{jk}s are close to the true values, which is expected since $\hat{\alpha}_{jk}$ is an unbiased estimator of α_{jk}. Note also that while the coverage probabilities of the nominally 95% confidence intervals ($\text{CP}_{95\%}$) for the β_{jk}s seem to be satisfactory (i.e., they are close to 0.95), the $\text{CP}_{95\%}$ for the α_{jk}s are far from the assumed levels. This difference may occur because we are considering that the asymptotic normality of the MLEs was achieved. However, this may not be true, returning inadequate confidence intervals. In order to overcome such a problem, in the next section, we will discuss an improved estimator for β_{jk}, as well as exact confidence intervals for both α_{jk} and β_{jk}.

V. BIAS CORRECTION AND IMPROVED CONFIDENCE INTERVALS

Cox and Snell [39] showed that, when the sample data are independent (although not necessarily identically distributed), the bias of $\hat{\theta}_w$, for $w = 1, \ldots, \kappa$, can be written as

$$\text{Bias}\left(\hat{\theta}_w\right) = \sum_{i=1}^{\kappa}\sum_{j=1}^{\kappa}\sum_{l=1}^{\kappa} s_{wi}(\boldsymbol{\theta}) s_{jl}(\boldsymbol{\theta}) \left(h_{ij,l}(\boldsymbol{\theta}) + 0.5 h_{ijl}(\boldsymbol{\theta})\right) + O(n^{-2}), \tag{16}$$

where s_{ij} is the (i, j)-th element of the variance-covariance matrix of $\hat{\boldsymbol{\theta}}$,

$$h_{ijl}(\boldsymbol{\theta}) = \mathbb{E}\left[\frac{\partial^3 \log L(\boldsymbol{\theta})}{\partial\theta_i \partial\theta_j \partial\theta_l}\right]$$

and

$$h_{ij,l}(\boldsymbol{\theta}) = \mathbb{E}\left[\frac{\partial^2 \log L(\boldsymbol{\theta})}{\partial\theta_i \partial\theta_j} . \frac{\partial \log L(\boldsymbol{\theta})}{\partial\theta_l}\right], \text{ for } i, j, l = 1, \ldots, \kappa.$$

Cordeiro and Klein [40] proved that, even when the data are dependent, the bias expression (16) can be rewritten as

$$\text{Bias}\left(\hat{\theta}_w\right) = \sum_{i=1}^{\kappa} s_{wi}(\boldsymbol{\theta}) \sum_{j=1}^{\kappa}\sum_{l=1}^{\kappa} s_{jl}(\boldsymbol{\theta}) \left(h_{ij}^{(l)}(\boldsymbol{\theta}) - 0.5 h_{ijl}(\boldsymbol{\theta})\right) + O(n^{-2}),$$

where $h_{ij}^{(l)}(\boldsymbol{\theta}) = \dfrac{\partial h_{ij}(\boldsymbol{\theta})}{\partial\theta_l}$, for $i, j, l = 1, \ldots, \kappa$.

Firth [41] showed that the first-order term is removed from the asymptotic bias of the MLEs by considering the Jeffreys prior [42] as a penalty function in the likelihood equation for the exponential family of distributions. The Jeffreys prior can be obtained as the square root of the determinant of the expected Fisher information matrix $I(\boldsymbol{\theta})$. Thus, it follows from equation (14) that

$$\begin{aligned}\pi^{\text{J}}(\boldsymbol{\theta}) &\propto |I(\boldsymbol{\theta})|^{1/2} \\ &= \sqrt{|\,\text{Diag}(\alpha_{11}\beta_{11}^{-2}, \ldots, \alpha_{1n_1}\beta_{1n_1}^{-2}, \ldots, \alpha_{p1}^{-1} \ldots, \alpha_{pn_p}^{-1})|} \\ &= \prod_{j=1}^{p}\prod_{k=1}^{n_j} \frac{1}{\beta_{jk}}.\end{aligned} \tag{17}$$

Note that after some algebraic manipulation, the likelihood function (10) can be rewritten as

$$L(\boldsymbol{\theta} \mid \boldsymbol{t}, \boldsymbol{\delta}, \boldsymbol{\psi}) \propto \prod_{j=1}^{p}\prod_{k=1}^{n_j} \gamma(\beta_{jk} \mid n_{jk} + 1, n_{jk}/\hat{\beta}_{jk}) \times \gamma(\alpha_{jk} \mid n_{jk} + 1, 1).$$

The marginal distribution for each parameter is independent of the other parameters. Moreover, since the marginals

TABLE 1: Bias, MSE and $CP_{95\%}$ from the MLEs, considering different parameter values (Scenarios 1, 2 and 3) and $M = 50,000$ simulated samples.

Scenario 1				Scenario 2				Scenario 3			
Parameter	Bias	MSE	$CP_{95\%}$	Parameter	Bias	MSE	$CP_{95\%}$	Parameter	Bias	MSE	$CP_{95\%}$
$\beta_{11} = 0.80$	0.408	2.430	0.955	$\beta_{11} = 1.20$	0.099	0.406	0.955	$\beta_{11} = 1.20$	0.144	0.579	0.955
$\beta_{12} = 0.50$	0.327	1.349	0.953	$\beta_{12} = 0.90$	0.112	0.409	0.955	$\beta_{12} = 1.10$	0.098	0.394	0.955
$\beta_{13} = 1.00$	0.214	0.841	0.956	$\beta_{13} = 1.00$	0.102	0.407	0.954	$\beta_{13} = 1.20$	0.115	0.459	0.954
$\beta_{21} = 1.00$	0.420	1.608	0.955	$\beta_{21} = 1.00$	0.436	1.874	0.955	$\beta_{21} = 1.50$	0.095	0.431	0.954
$\beta_{22} = 1.00$	0.692	3.120	0.953	$\beta_{22} = 2.00$	0.109	0.527	0.952	$\beta_{22} = 1.80$	0.091	0.452	0.950
$\beta_{23} = 1.10$	0.625	2.596	0.952	$\beta_{23} = 1.20$	0.138	0.531	0.953	$\beta_{23} = 1.60$	0.165	0.650	0.954
$\alpha_{11} = 3.30$	0.485	1.642	0.998	$\alpha_{11} = 14.56$	-0.015	3.815	0.945	$\alpha_{11} = 10.92$	-0.007	3.302	0.908
$\alpha_{12} = 2.23$	0.813	1.425	0.997	$\alpha_{12} = 10.37$	0.022	3.220	0.936	$\alpha_{12} = 13.49$	-0.004	3.663	0.948
$\alpha_{13} = 7.00$	0.053	2.611	0.919	$\alpha_{13} = 12.00$	0.008	3.450	0.944	$\alpha_{13} = 12.74$	-0.003	3.557	0.927
$\alpha_{21} = 4.00$	0.325	1.829	0.997	$\alpha_{21} = 4.00$	0.325	1.822	0.997	$\alpha_{21} = 17.89$	-0.033	4.217	0.932
$\alpha_{22} = 2.00$	0.900	1.404	0.998	$\alpha_{22} = 20.00$	0.005	4.494	0.946	$\alpha_{22} = 21.97$	0.024	4.692	0.942
$\alpha_{23} = 2.00$	0.659	1.509	0.997	$\alpha_{23} = 10.92$	-0.012	3.284	0.910	$\alpha_{23} = 12.07$	-0.022	3.467	0.948

TABLE 2: Bias, MSE and $CP_{95\%}$ from the MLEs, considering different parameter values (Scenarios 4, 5 and 6) and $M = 50,000$ simulated samples.

Scenario 4				Scenario 5				Scenario 6			
Parameter	Bias	MSE	$CP_{95\%}$	Parameter	Bias	MSE	$CP_{95\%}$	Parameter	Bias	MSE	$CP_{95\%}$
$\beta_{11} = 2.00$	0.349	1.316	0.955	$\beta_{11} = 0.80$	0.308	1.193	0.956	$\beta_{11} = 2.00$	0.346	1.263	0.954
$\beta_{12} = 0.40$	0.135	0.550	0.955	$\beta_{12} = 0.80$	0.137	0.537	0.955	$\beta_{12} = 1.10$	0.029	0.188	0.952
$\beta_{21} = 0.60$	0.061	0.239	0.955	$\beta_{21} = 0.60$	0.095	1.111	0.956	$\beta_{21} = 1.20$	0.017	0.146	0.951
$\beta_{22} = 0.70$	0.071	0.279	0.956	$\beta_{22} = 0.30$	0.105	0.377	0.954	$\beta_{22} = 1.10$	0.028	0.186	0.951
$\beta_{23} = 1.50$	0.225	0.863	0.956	$\beta_{23} = 1.10$	0.190	0.868	0.956	$\beta_{23} = 1.50$	0.228	0.879	0.956
$\beta_{31} = 0.40$	0.053	0.205	0.955	$\beta_{31} = 0.50$	0.079	0.432	0.957	$\beta_{31} = 1.10$	0.013	0.126	0.952
$\beta_{32} = 0.80$	0.153	0.705	0.956	$\beta_{32} = 1.30$	0.262	0.942	0.957	$\beta_{32} = 1.20$	0.052	0.270	0.951
$\alpha_{11} = 8.00$	0.019	2.799	0.894	$\alpha_{11} = 4.39$	0.265	1.953	0.993	$\alpha_{11} = 8.00$	0.011	2.808	0.893
$\alpha_{12} = 4.97$	0.172	2.109	0.904	$\alpha_{12} = 8.24$	0.016	2.854	0.909	$\alpha_{12} = 40.48$	0.008	6.325	0.953
$\alpha_{21} = 12.07$	-0.020	3.480	0.948	$\alpha_{21} = 9.05$	-0.004	3.005	0.941	$\alpha_{21} = 72.82$	0.058	8.484	0.951
$\alpha_{22} = 12.21$	-0.019	3.488	0.910	$\alpha_{22} = 4.67$	0.217	2.019	0.996	$\alpha_{22} = 40.48$	0.017	6.396	0.950
$\alpha_{23} = 8.94$	0.033	2.958	0.942	$\alpha_{23} = 8.10$	0.024	2.828	0.900	$\alpha_{23} = 8.94$	-0.006	2.980	0.938
$\alpha_{31} = 9.94$	-0.014	3.146	0.923	$\alpha_{31} = 8.94$	-0.015	2.981	0.939	$\alpha_{31} = 80.96$	-0.009	8.978	0.944
$\alpha_{32} = 7.69$	0.019	2.747	0.945	$\alpha_{32} = 7.37$	0.042	2.683	0.931	$\alpha_{32} = 25.49$	-0.005	5.028	0.938

TABLE 3: Bias, MSE and $CP_{95\%}$ from the CMLEs, considering different parameter values (Scenarios 1, 2 and 3) and $M = 50,000$ simulated samples.

Scenario 1				Scenario 2				Scenario 3			
Parameter	Bias	MSE	$CP_{95\%}$	Parameter	Bias	MSE	$CP_{95\%}$	Parameter	Bias	MSE	$CP_{95\%}$
$\beta_{11} = 0.80$	0.004	1.262	0.950	$\beta_{11} = 1.20$	0.001	0.358	0.951	$\beta_{11} = 1.20$	0.003	0.459	0.949
$\beta_{12} = 0.50$	0.003	0.691	0.949	$\beta_{12} = 0.90$	0.001	0.337	0.951	$\beta_{12} = 1.10$	0.001	0.344	0.952
$\beta_{13} = 1.00$	-0.001	0.564	0.950	$\beta_{13} = 1.00$	-0.001	0.347	0.950	$\beta_{13} = 1.20$	0.001	0.396	0.950
$\beta_{21} = 1.00$	-0.001	0.896	0.950	$\beta_{21} = 1.00$	0.006	1.012	0.950	$\beta_{21} = 1.50$	-0.001	0.392	0.951
$\beta_{22} = 1.00$	0.005	1.568	0.951	$\beta_{22} = 2.00$	-0.003	0.486	0.951	$\beta_{22} = 1.80$	0.000	0.419	0.947
$\beta_{23} = 1.10$	-0.007	1.347	0.951	$\beta_{23} = 1.20$	-0.001	0.441	0.949	$\beta_{23} = 1.60$	0.001	0.550	0.949
$\alpha_{11} = 3.30$	0.485	1.642	0.940	$\alpha_{11} = 14.56$	-0.015	3.815	0.935	$\alpha_{11} = 10.92$	-0.007	3.302	0.954
$\alpha_{12} = 2.23$	0.813	1.425	0.960	$\alpha_{12} = 10.37$	0.022	3.220	0.911	$\alpha_{12} = 13.49$	-0.004	3.663	0.924
$\alpha_{13} = 7.00$	0.053	2.611	0.973	$\alpha_{13} = 12.00$	0.008	3.450	0.942	$\alpha_{13} = 12.74$	-0.003	3.557	0.952
$\alpha_{21} = 4.00$	0.325	1.829	0.944	$\alpha_{21} = 4.00$	0.325	1.822	0.945	$\alpha_{21} = 17.89$	-0.033	4.217	0.958
$\alpha_{22} = 2.00$	0.900	1.404	0.914	$\alpha_{22} = 20.00$	0.005	4.494	0.944	$\alpha_{22} = 21.97$	0.024	4.692	0.958
$\alpha_{23} = 2.00$	0.659	1.509	0.914	$\alpha_{23} = 10.92$	-0.012	3.284	0.944	$\alpha_{23} = 12.07$	-0.022	3.467	0.958

follow a gamma distribution, they belong to the exponential family of distributions. Hence, the approach proposed by Firth [41] is valid for our hierarchical competing risks model. The penalized log-likelihood function using the Jeffreys prior (17) as a penalized criterion can be written as

$$L_{\mathrm{P}}(\boldsymbol{\theta} \mid \boldsymbol{t}, \boldsymbol{\delta}, \boldsymbol{\psi}) \propto \prod_{j=1}^{p} \prod_{k=1}^{n_j} \gamma(\beta_{jk} \mid n_{jk}, n_{jk}/\hat{\beta}_{jk}) \times \gamma(\alpha_{jk} \mid n_{jk}+1, 1),$$

Then, with some algebraic manipulation, we obtain the corrected MLEs (CMLEs) given by

$$\tilde{\beta}_{jk} = \frac{n_{jk}-1}{n_{jk}} \hat{\beta}_{jk} \tag{18}$$

and

$$\tilde{\alpha}_{jk} = \hat{\alpha}_{jk}, \tag{19}$$

which are unbiased to $O(n_{jk}^{-1})$. Although the penalized likelihood method introduced by Firth [41] only ensures that the first-order term is removed from the asymptotic bias, we have that

$$\mathbb{E}\left[\tilde{\beta}_{jk} \mid \boldsymbol{t}, \boldsymbol{\delta}, \boldsymbol{\psi}\right] = \beta_{jk}$$

and

$$\mathbb{E}\left[\tilde{\alpha}_{jk} \mid \boldsymbol{t}, \boldsymbol{\delta}, \boldsymbol{\psi}\right] = \alpha_{jk}.$$

Therefore, the obtained CMLEs are unbiased for $n_{jk} > 1$.

As we observed from the simulation results presented in Section IV-A, the asymptotic confidence intervals are not satisfactory for small samples. Using the improved estimates in the estimators of the asymptotic variance, which are used to obtain the confidence intervals, will return the worst results in terms of coverage probabilities than obtained with the MLEs. On the other hand, by observing that

$$L_{\mathrm{P}}(\alpha_{jk} \mid \boldsymbol{t}, \boldsymbol{\delta}, \boldsymbol{\psi}) = \frac{\alpha_{jk}^{n_{jk}} e^{-\alpha_{jk}}}{n_{jk}!},$$

i.e., $\alpha_{jk} \sim \text{Erlang}(n_{jk}+1, 1)$, then $2\alpha_{jk} \sim \chi^2_{2(n_{jk}+1)}$. Therefore, the $100(1-\xi)\%$ confidence interval for α_{jk} can be calculated as

$$\left[\frac{1}{2}\chi^2_{2n_{jk}+2;\,\xi/2}\,;\,\frac{1}{2}\chi^2_{2n_{jk}+2;\,1-\xi/2}\right], \tag{20}$$

where $\chi^2_{a;\,\upsilon}$ represents the 100υ-th percentile of the chi-square distribution with a degrees of freedom.

Furthermore, since $L_{\mathrm{P}}(\beta_{jk} \mid \boldsymbol{t}, \boldsymbol{\delta}, \boldsymbol{\psi}) = \gamma(\beta_{jk} \mid n_{jk}, n_{jk}/\hat{\beta}_{jk})$, we have that the $100(1-\xi)\%$ confidence interval for β_{jk} can be obtained directly from the quantile function of the gamma distribution, that is,

$$\left[\gamma_{\mathrm{Q}}\left(n_{jk}, n_{jk}/\hat{\beta}_{jk};\, \xi/2\right)\,;\,\gamma_{\mathrm{Q}}\left(n_{jk}, n_{jk}/\hat{\beta}_{jk};\, 1-\xi/2\right)\right], \tag{21}$$

where $\gamma_{\mathrm{Q}}(a, b; \upsilon)$ is the quantile function of the gamma distribution with shape parameter a and scale parameter b, and $0 \leq \upsilon \leq 1$. This quantile function is available in most of the standard statistical softwares. For instance, in R it can be computed by using the *qgamma(.)* function. Thus, the exact confidence intervals for the model parameters can be obtained without the use of intensive computation.

A. SIMULATION STUDY

In this section, we perform a second simulation study with the same general specifications (i.e., same scenarios, number of Monte Carlo replications and evaluation criteria) of the first one shown in Section IV-A. However, the main goal now is to assess the performance (i.e., the consistency and efficiency) of the CMLEs for the model parameters presented in equations (18) and (19), as well as of the exact confidence intervals given in equations (20) and (21). It is worthwhile mentioning that the generated samples are the same as those of Section IV-A, in order to achieve a fair comparison of the different approaches.

Tables 1, 2, 3 and 4 summarize the results. The CMLEs of the β_{jk}s are more adequate, since their bias were successfully removed compared with their corresponding MLEs. Moreover, the $\mathrm{CP}_{95\%}$ for the α_{jk}s using the exact confidence intervals, rather than the asymptotic confidence intervals, are in general higher and closer to the nominal value (0.95).

VI. APPLICATIONS

In this section, we illustrate the usefulness of the new methodology considering three data sets: an artificial data set for a butterfly valve system (Section VI-A), a data set from a real early-stage project of an in-pipe robot traction system (Section VI-B), and a real data set consisting of failures of a blowout preventer system (Section VI-C).

A. BUTTERFLY VALVE SYSTEM: A TOY EXAMPLE

To illustrate the inference process in hierarchical competing risks model, we start with a toy example based on a butterfly valve system. Butterfly valves are exact, low cost and a lightweight valve with excellent capability and durability, consisting of fewer parts, which makes butterfly valves easy to maintain, repair and less structural support for productive use [35]. They contain a disc, which is positioned in the center that can be rotated a quarter of a turn through a shaft running. For this reason, this kind of valve is known as quarter-turn valves [43]. The rotation of the disc determines the flow passing a pipe, whose maximum occurs when the disc is positioned parallel to the stream and minimum when perpendicular to it. The relative position between the geometric center of the disc and the shaft defines if the valve is namely symmetrical, eccentric or double eccentric [44].

Butterfly valves include a wide range of applications with excellent isolation, throttling as well as on-off service and flow regulation [45]. They provide reliable, long-term performance that satisfies a wide range of industrial applications such as oil and gas. For instance, the applications involve isolation or regulating of oil and gas equipment, fill and drain or bypass systems and other similar applications where the principal function for the control of the flow or pressure can be satisfied whether on or off [46].

TABLE 4: Bias, MSE and $CP_{95\%}$ from the CMLEs, considering different parameter values (Scenarios 4, 5 and 6) and $M = 50,000$ simulated samples.

Scenario 4				Scenario 5				Scenario 6			
Parameter	Bias	MSE	$CP_{95\%}$	Parameter	Bias	MSE	$CP_{95\%}$	Parameter	Bias	MSE	$CP_{95\%}$
$\beta_{11} = 2.00$	-0.003	0.960	0.950	$\beta_{11} = 0.80$	0.001	0.678	0.950	$\beta_{11} = 2.00$	-0.008	0.939	0.950
$\beta_{12} = 0.40$	0.000	0.314	0.951	$\beta_{12} = 0.80$	0.000	0.380	0.949	$\beta_{12} = 1.10$	0.001	0.181	0.950
$\beta_{21} = 0.60$	0.000	0.205	0.951	$\beta_{21} = 0.60$	0.002	0.588	0.950	$\beta_{21} = 1.20$	0.000	0.143	0.950
$\beta_{22} = 0.70$	0.000	0.236	0.952	$\beta_{22} = 0.30$	-0.002	0.222	0.951	$\beta_{22} = 1.10$	-0.001	0.179	0.950
$\beta_{23} = 1.50$	-0.001	0.658	0.950	$\beta_{23} = 1.10$	-0.002	0.581	0.950	$\beta_{23} = 1.50$	-0.001	0.658	0.950
$\beta_{31} = 0.40$	0.000	0.163	0.950	$\beta_{31} = 0.50$	0.002	0.271	0.952	$\beta_{31} = 1.10$	-0.001	0.124	0.952
$\beta_{32} = 0.80$	0.002	0.476	0.950	$\beta_{32} = 1.30$	0.002	0.671	0.951	$\beta_{32} = 1.20$	0.000	0.254	0.949
$\alpha_{11} = 8.00$	0.019	2.799	0.957	$\alpha_{11} = 4.39$	0.265	1.953	0.961	$\alpha_{11} = 8.00$	0.011	2.808	0.954
$\alpha_{12} = 4.97$	0.172	2.109	0.968	$\alpha_{12} = 8.24$	0.016	2.854	0.949	$\alpha_{12} = 40.48$	0.008	6.325	0.944
$\alpha_{21} = 12.07$	-0.020	3.480	0.940	$\alpha_{21} = 9.05$	-0.004	3.005	0.937	$\alpha_{21} = 72.82$	0.058	8.484	0.949
$\alpha_{22} = 12.21$	-0.019	3.488	0.940	$\alpha_{22} = 4.67$	0.217	2.019	0.949	$\alpha_{22} = 40.48$	0.017	6.396	0.941
$\alpha_{23} = 8.94$	0.033	2.958	0.942	$\alpha_{23} = 8.10$	0.024	2.828	0.952	$\alpha_{23} = 8.94$	-0.006	2.980	0.939
$\alpha_{31} = 9.94$	-0.014	3.146	0.965	$\alpha_{31} = 8.94$	-0.015	2.981	0.940	$\alpha_{31} = 80.96$	-0.009	8.978	0.950
$\alpha_{32} = 7.69$	0.019	2.747	0.960	$\alpha_{32} = 7.37$	0.042	2.683	0.944	$\alpha_{32} = 25.49$	-0.005	5.028	0.955

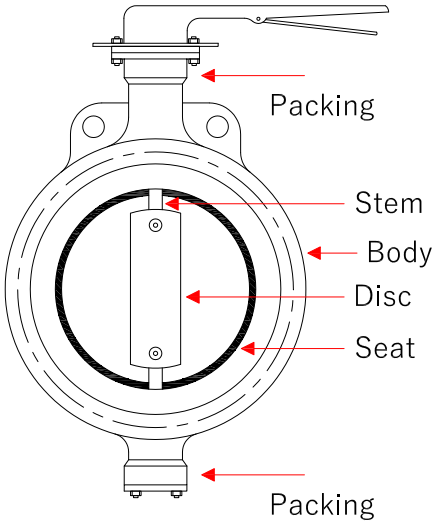

FIGURE 3: Schematic diagram of a butterfly valve.

As shown in Figure 3, the butterfly valve includes a disc valve, placed inside one configured valve body that rotates about its axis separate from the axis of rotation of the stems that support the disc valve in position for a turn between opening and closure. A packing part is located connecting the valve body and the stem to prevent any leakage happening when the flow passes into the pipe. Furthermore, a ring seal acts as a seal between the metal disc and body to avoid any leakage when the valve is in the fully closed position.

Because of the critical impact of the butterfly valve in the industry, in this paper, the attention is focused on carrying an FTA to increase the performance of this type of valve. The main goal is to know the failures and with new maintenance limits or avoid different risks within the valve performance. Hence, the FTA moves towards higher reliability, higher quality, and improved safety. As can be seen in Figure 4, we created the FTA based on the Failure Mode and Effects Analysis (FMEA) available in Bin and Abdullah [35], with reviewing primary components of the butterfly valve, which consists of a body, metal, disc, stem, seat and packing with several failure modes and their causes. It is worthwhile mentioning that these failures happen due to one of the series competing failure mechanisms, whereby each of them act related to the system independently. Based on the information provided in the FMEA by Bin and Abdullah [35], we were able to generate the data set, as shown in Table 5, which is representative of a butterfly valve system. Two numbers represent the failure modes, say 1.1, the first one stands for the system, in our example, system 1, and the second number stands for the sub-system, in our example, sub-system 1. Furthermore, we can evaluate the proportion of the PLP for each cause of failure by employing a graphical tool, which is known as the Duane plot [19]. As can be seen in Figure 5, the values of the sub-systems are close to the line. This means that the obtained data set comes from a PLP, and our approach can be adequately used.

Table 6 displays the bias-corrected maximum likelihood (CML) estimates, along with the corresponding 95% exact confidence intervals (CI 95%) for the model parameters. The results shown in this table suggest that the reliability of the body and stem components improve over time since the corresponding $\hat{\beta}_{1k}$s and $\hat{\beta}_{3k}$s are less than one. Moreover, observe that the reliability of the disk components may decrease over time due to corrosion on the disk surface ($\hat{\beta}_{22} = 1.535 > 1$), while the reliability of the seat and packing components show an intermediate behavior since their CML estimates are close to one. Note, however, that almost all the CI 95% include the one. Therefore, we can not say that the cause-specific intensity functions of some components increase or decrease over time.

It is essential to point out that such results can provide valuable insights to the maintenance crew. They also allow

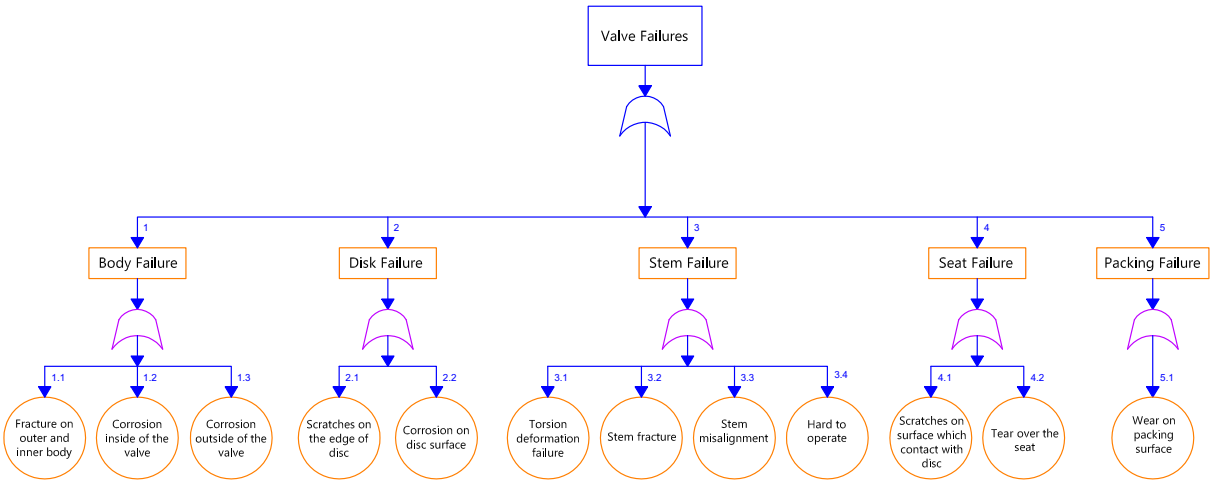

FIGURE 4: FTA of butterfly valve failure.

TABLE 5: Failure data for a butterfly valve.

Failure Time	Failure Mode	Failure Time	Failure Mode	Failure Time	Failure Mode
32.03	1.1	10.38	1.3	46.54	4.1
7.37	1.1	57.37	2.1	33.63	4.1
4.38	1.1	2.68	2.1	25.58	4.1
44.35	1.1	13.24	2.1	20.84	4.1
30.00	1.1	15.45	2.1	39.87	4.1
0.41	1.2	12.42	2.2	22.17	4.1
1.71	1.2	50.39	2.2	4.91	4.1
45.86	1.2	56.48	2.2	57.63	4.1
0.13	1.2	47.89	2.2	26.00	4.2
16.41	1.2	33.93	2.2	31.30	4.2
17.40	1.2	1.52	3.1	51.34	4.2
36.61	1.2	48.39	3.1	8.38	4.2
0.22	1.2	3.55	3.2	44.89	5.1
47.98	1.3	43.97	3.2	35.09	5.1
4.98	1.3	10.46	3.3	48.25	5.1
8.71	1.3	37.14	3.3	11.46	5.1
59.46	1.3	24.93	3.4	9.22	5.1
7.87	1.3	4.68	3.4	48.59	5.1
41.67	1.3	33.72	3.4	35.95	5.1

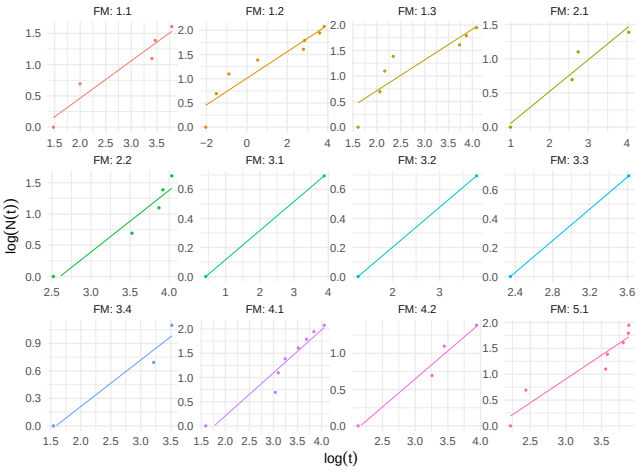

FIGURE 5: Duane plots for the failure modes of a butterfly valve.

us to estimate the intensity function of each system or sub-system and the hazard function of the overall system. The estimated intensity functions can be obtained from (4), while the overall hazard function can be obtained from (5), with the parameters substituted by their estimates. Table 7 presents the estimated intensity functions for each sub-system and the estimated hazard function over some fixed failure times. Observe that the results shown in this table are in agreement with the ones presented in Table 6, that is, for the cases where $\hat{\beta}_{jk} > 1$ the intensity function increases over time, while for $\hat{\beta}_{jk} < 1$ the intensity function decreases over time. We also see that the overall hazard function decreases over time, which may be due to the repair and maintenance effects.

In order to provide a better understanding of the effect of fatigue damage on any point of the butterfly valve components, we then created a fatigue simulation, which is given as follows. Fatigue design of the butterfly valve is done using design fatigue curves, which are created based on the relationship between fatigue life and stress or strain. Because in the real structure of the valve, its components are constantly subjected to the high cycle fatigue stress and therefore, cracks begin from regions of concentrated stress resulting from this cycle fatigue and corresponding fatigue safety factor [47]. It is thus essential to determine the safety factor of fatigue failure, which indicates the ability of damage in the critical area in the valve components. The safety factor for this valve is determined by evaluating the effects of the loading history due to the fluid-structure interaction on fatigue life [48]. All computations and simulations required to build Figures 6 and 7 were performed with coupling CFD (fluids) and FEM (mechanics) models, which were prepared using the commercial pieces of software FLUENT and ANSYS 2019 R1. Figure 6 shows the safety factor of fatigue life associated with any point of the butterfly valve components. As can be

TABLE 6: CML estimates and CI 95% of parameters β_{jk} and α_{jk}, considering the butterfly valve failure data.

Parameter	Estimate	CI 95%
β_{11}	0.631	[0.256 ; 1.616]
β_{12}	0.297	[0.146 ; 0.612]
β_{13}	0.682	[0.320 ; 1.484]
β_{21}	0.498	[0.181 ; 1.456]
β_{22}	1.535	[0.623 ; 3.931]
β_{31}	0.257	[0.062 ; 1.432]
β_{32}	0.319	[0.077 ; 1.775]
β_{33}	0.449	[0.109 ; 2.502]
β_{34}	0.499	[0.154 ; 1.804]
β_{41}	1.046	[0.516 ; 2.156]
β_{42}	0.831	[0.302 ; 2.428]
β_{51}	1.133	[0.531 ; 2.466]
α_{11}	5.000	[2.202 ; 11.668]
α_{12}	8.000	[4.115 ; 15.763]
α_{13}	7.000	[3.454 ; 14.423]
α_{21}	4.000	[1.623 ; 10.242]
α_{22}	5.000	[2.202 ; 11.668]
α_{31}	2.000	[0.619 ; 7.225]
α_{32}	2.000	[0.619 ; 7.225]
α_{33}	2.000	[0.619 ; 7.225]
α_{34}	3.000	[1.090 ; 8.767]
α_{41}	8.000	[4.115 ; 15.763]
α_{42}	4.000	[1.623 ; 10.242]
α_{51}	7.000	[3.454 ; 14.423]

TABLE 7: Estimates of the subsystem-specific and overall intensity functions at different times, considering the butterfly valve failure data.

Intensity	Time (months)				
	5	15	25	40	55
λ_{11}	0.132	0.088	0.073	0.061	0.054
λ_{12}	0.227	0.105	0.073	0.053	0.042
λ_{13}	0.175	0.124	0.105	0.091	0.082
λ_{21}	0.116	0.067	0.052	0.041	0.035
λ_{22}	0.034	0.061	0.080	0.103	0.122
λ_{31}	0.054	0.024	0.016	0.012	0.009
λ_{32}	0.058	0.027	0.019	0.014	0.011
λ_{33}	0.059	0.032	0.024	0.019	0.016
λ_{34}	0.087	0.050	0.039	0.031	0.026
λ_{41}	0.124	0.131	0.134	0.137	0.139
λ_{42}	0.084	0.070	0.064	0.059	0.056
λ_{51}	0.095	0.110	0.118	0.125	0.131
λ	1.245	0.888	0.797	0.744	0.723

seen, the safety factor values are presented in terms of change between 0 and 15, in which the lower value identifies the critical damage locations in the component. Analysis over the safety factor of fatigue life results revealed that fatigue could be expected to initiate near the stems, due to their role as stress concentration points. It can be observed that the butterfly valve has several components connected in series. Therefore, a single component failure results in total system failure. The available fatigue life curve, in cycles, for the estimation of a finite lifetime of the butterfly valve under 50% to 100% of the fatigue loading history, is presented in Figure 7. Analysis of the outcomes shows how the fatigue results change as a function of the loading at the critical location on the model. For instance, the results from this figure verified that the minimum value of fatigue life appeared at the maximum fatigue loading of 100%. Therefore, damage starts from the points related to the component with the lowest fatigue safety factor due to the significant stress concentration. Finally, as a conclusion, a good comparison was observed between the simulated fatigue damage results and statistical analysis. However, the present safety factor fatigue simulation indicates some disagreement, which is possibly related to differences in conditions between this simulation and statistical analysis.

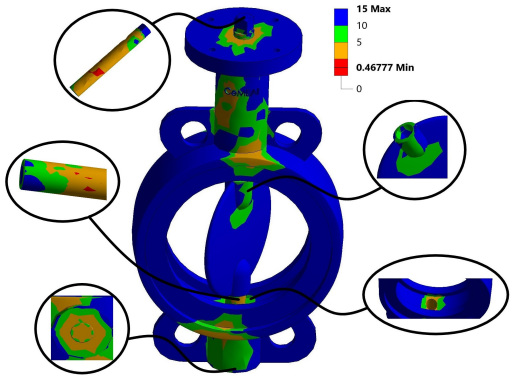

FIGURE 6: Fatigue safety factors of the butterfly valve components.

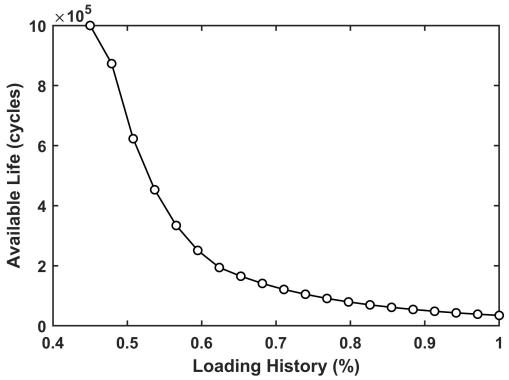

FIGURE 7: Available fatigue life of the butterfly valve components.

B. IN-PIPE ROBOT TRACTION SYSTEM: EXAMPLE ON EARLY-STAGE INNOVATIVE PROJECT

In this section, we consider another example based on a real problem we are working on in a partnership with Petrobras (abbreviation of *Petróleo Brasileiro S.A.*), which is the Brazil's largest oil and gas producer. The problem is related to the traction system of an in-pipe robot that was developed, though still in its early stage of development, to be used at a future time to remove hydrates that form in pipelines and can cause problems in oil and gas flow. In this case, a locomotive

is responsible for conducting the robot inside the pipe, and once hydrate formation is identified, the robot will work on its safe removal for the oil to flow again. A schematic of the studied system is shown in Figure 8.

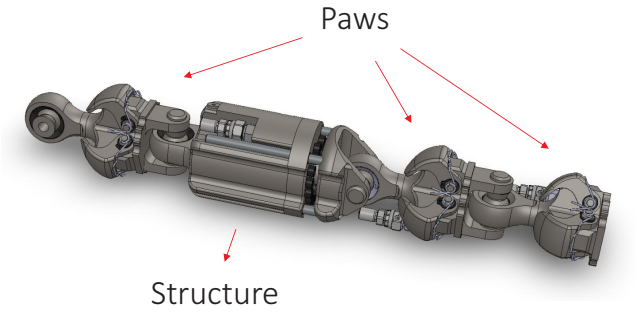

FIGURE 8: Schematic diagram of an in-pipe robot traction system.

We obtained a suitable data set for this problem using a similar approach as proposed in the previous section, i.e., based on the limited but available information provided by FMEA and FTA tools. Due to the criticality of the traction system, we will focus on it instead of the overall locomotive system. An excerpt from the FMEA devised by the project executing team is shown in Table 8. On the other hand, the hierarchy of failure modes that compete with each other to cause a general system failure can be seen in Figure 9. Thus, these two tools supported the generation of the data set shown in Table 9, whose parameter representativeness tries to express the degree of severity and occurrence of the FMEA used.

TABLE 8: FMEA for the in-pipe robot traction system. S = Severity, O = Occurrence, D = Detection.

General System	System	Failure Mode	S	O	D
Mechanical components	Paws	Compromised paw lining adhesive	7	3	3
		No arms retraction	9	3	9
		Paw slip	9	3	9
		Riser deformation	9	3	9
		Riser rupture	9	1	9
		Rubber coating degradation	7	3	7
	Structure	Cracking by atomic hydrogen permeation	9	9	9
		Stress concentration	9	5	9

Duane plots applied to the data for each failure mode show evidence that a PLP may be able to adequately describe the behavior of system-associated failure times, since the scattered points show an approximately linear trend (see Figure 10).

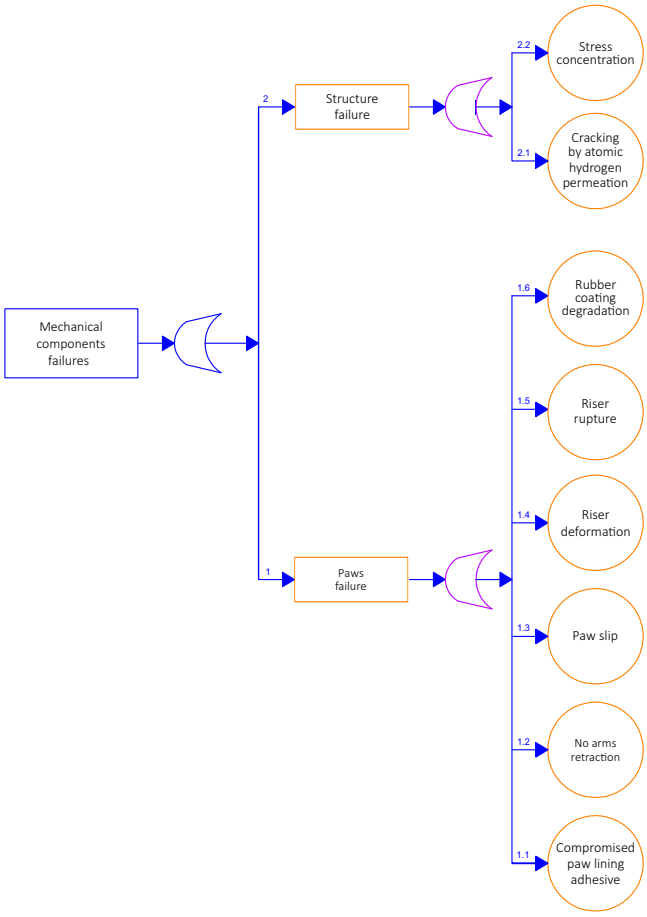

FIGURE 9: FTA of in-pipe robot traction system failure.

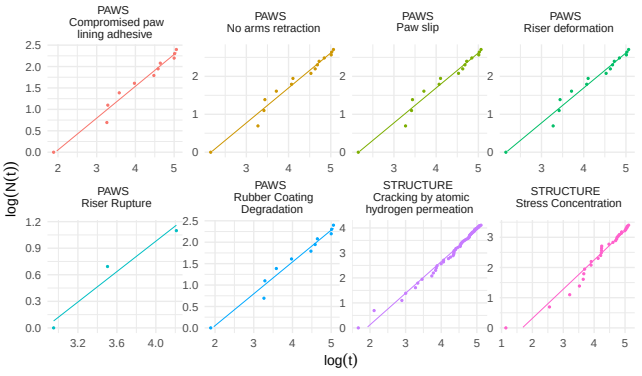

FIGURE 10: Duane plots for the failure modes related to the in-pipe robot traction system.

The CML estimates for the parameters associated with each failure mode, as well as their respective CI 95%, are presented in Table 10. From these results, there is evidence that the intensity associated with some failure modes (e.g., *Cracking by atomic hydrogen permeation*) increases. On the other hand, there seems to be a decrease in risks associated with other failure modes (e.g., *Compromised paw lining adhesive* and *Riser rupture*), although their CI 95% contains

TABLE 9: Failure data for the in-pipe robot traction system. FT = Failure Time, FM = Failure Mode.

FT	FM	FT	FM	FT	FM	FT	FM	FT	FM	FT	FM
36.0	1.1	112.6	1.3	150.2	1.6	119.2	2.1	90.1	2.1	38.3	2.2
53.2	1.1	60.6	1.3	26.1	1.6	31.9	2.1	69.6	2.1	152.2	2.2
87.9	1.1	127.1	1.3	148.3	1.6	58.4	2.1	119.1	2.1	159.4	2.2
150.2	1.1	79.8	1.3	157.2	1.6	78.4	2.1	56.8	2.1	114.6	2.2
26.1	1.1	117.9	1.3	103.8	1.6	5.3	2.1	93.1	2.1	109.5	2.2
148.3	1.1	166.6	1.3	98.0	1.6	77.8	2.1	135.8	2.1	12.8	2.2
157.2	1.1	59.9	1.3	6.6	1.6	150.2	2.1	23.2	2.1	39.0	2.2
103.8	1.1	128.5	1.3	26.8	1.6	70.9	2.1	151.0	2.1	33.9	2.2
98.0	1.1	40.9	1.4	22.4	1.6	93.7	2.1	70.7	2.1	118.8	2.2
6.6	1.1	58.6	1.4	108.6	1.6	111.6	2.1	146.0	2.1	69.4	2.2
26.8	1.1	92.8	1.4	55.2	1.6	95.5	2.1	72.0	2.1	131.9	2.2
40.9	1.2	151.6	1.4	124.0	1.6	43.8	2.1	69.8	2.1	88.2	2.2
58.6	1.2	30.5	1.4	74.7	1.6	144.4	2.1	92.8	2.1	123.7	2.2
92.8	1.2	149.9	1.4	114.2	1.6	121.7	2.1	153.3	2.1	166.7	2.2
151.6	1.2	158.1	1.4	166.4	1.6	139.7	2.1	149.5	2.1	68.8	2.2
30.5	1.2	108.0	1.4	54.6	1.6	28.3	2.1	79.1	2.1	133.2	2.2
149.9	1.2	102.5	1.4	125.4	1.6	129.7	2.1	137.3	2.1	157.8	2.2
158.1	1.2	8.6	1.4	155.3	1.6	82.5	2.1	162.7	2.1	40.1	2.2
108.0	1.2	31.2	1.4	58.1	2.1	143.5	2.1	86.2	2.1	113.1	2.2
102.5	1.2	26.4	1.4	76.1	2.1	118.6	2.1	128.1	2.1	24.7	2.2
8.6	1.2	112.6	1.4	107.6	2.1	138.1	2.1	80.7	2.1	49.7	2.2
31.2	1.2	60.6	1.4	155.5	2.1	104.6	2.1	68.4	2.1	69.8	2.2
26.4	1.2	127.1	1.4	46.6	2.1	101.0	2.1	134.5	2.1	3.1	2.2
112.6	1.2	79.8	1.4	154.2	2.1	139.0	2.1	46.8	2.1	69.1	2.2
60.6	1.2	117.9	1.4	160.5	2.1	8.3	2.1	127.9	2.1	147.7	2.2
127.1	1.2	166.6	1.4	120.6	2.1	92.9	2.1	31.1	2.1	62.1	2.2
79.8	1.2	59.9	1.4	115.9	2.1	130.9	2.1	54.6	2.1	85.6	2.2
117.9	1.2	128.5	1.4	18.1	2.1	125.2	2.1	35.5	2.1	104.7	2.2
40.9	1.3	19.1	1.5	47.4	2.1	93.0	2.1	53.5	2.1	87.5	2.2
58.6	1.3	33.2	1.5	41.9	2.1	149.1	2.1	17.4	2.1	35.6	2.2
92.8	1.3	67.4	1.5	124.4	2.1	86.8	2.1	117.9	2.1	141.0	2.2
151.6	1.3	143.5	1.5	78.1	2.1	54.5	2.1	151.1	2.1	115.8	2.2
30.5	1.3	12.2	1.5	136.3	2.1	20.1	2.1	137.5	2.1	135.8	2.2
149.9	1.3	140.9	1.5	96.1	2.1	26.5	2.1	140.1	2.1	21.5	2.2
158.1	1.3	153.0	1.5	128.8	2.1	66.9	2.1	89.5	2.1	124.6	2.2
108.0	1.3	85.2	1.5	166.9	2.1	99.3	2.1	82.3	2.1	74.0	2.2
102.5	1.3	78.6	1.5	77.4	2.1	120.8	2.1	49.4	2.2	140.0	2.2
8.6	1.3	36.0	1.6	137.3	2.1	81.8	2.1	67.4	2.2	112.4	2.2
31.2	1.3	53.2	1.6	159.2	2.1	156.2	2.1	100.4	2.2	134.0	2.2
26.4	1.3	87.9	1.6	48.6	2.1	63.0	2.1	153.7	2.2	97.2	2.2

the one.

TABLE 10: CML estimates and CI 95% of model parameters, considering the in-pipe robot traction system failure data.

Failure Mode	Parameter	Estimate	CI 95%
Compromised paw lining adhesive	β_{11}	0.862	[0.474 ; 1.586]
	α_{11}	11.000	[6.201 ; 19.682]
No arms retraction	β_{12}	1.047	[0.648 ; 1.700]
	α_{12}	17.000	[10.668 ; 27.219]
Paw slip	β_{13}	1.145	[0.736 ; 1.789]
	α_{13}	20.000	[12.999 ; 30.888]
Riser deformation	β_{14}	1.145	[0.736 ; 1.789]
	α_{14}	20.000	[12.999 ; 30.888]
Riser rupture	β_{15}	0.870	[0.448 ; 1.714]
	α_{15}	9.000	[4.795 ; 17.085]
Rubber coating degradation	β_{16}	1.101	[0.716 ; 1.700]
	α_{16}	21.000	[13.787 ; 32.101]
Cracking by atomic hydrogen permeation	β_{21}	1.390	[1.140 ; 1.696]
	α_{21}	98.000	[80.462 ; 119.431]
Stress concentration	β_{22}	1.232	[0.916 ; 1.659]
	α_{22}	44.000	[32.823 ; 59.068]

The behavior over time of the estimated intensities and reliabilities, for each specific failure mode, is shown in Figures 11a and 11b, from which we can see that the intensities associated with the failure modes 2.1 and 2.2 (*Structure* system) grow significantly more than others. In addition, the median lifespan of these sub-systems is around five weeks, while the rest is around seven weeks.

The combination of individual intensities and reliabilities, within their respective hierarchies, results in specific functions corresponding to each system. In this context, it is possible to study such measures by considering a level above in the hierarchy. The results are shown in Figure 11c, where it can be seen that the intensity of the *Paws* system grows significantly much less than the *Structure* system; however, in the (approximately) twenty initial weeks, its intensity is lower than the *Paws* system. This can also be observed from the reliability curve, where the median lifetime of the *Paws* system is around one week, while that of the *Structure* system is close to three. In addition, the curves become very close from week fifteen.

Finally, the combination of the intensities and reliabilities of all failure modes results in their respective functions for the general system, as a whole. Thus, there is a growing intensity associated with it, and a median time of operation close to one week.

C. BLOWOUT PREVENTER SYSTEM: A REAL EXAMPLE

A blowout preventer (BOP) is a large, specially designed valve that is used to seal, control and monitor oil and gas wells [49]. This valve mounts on top of the well during the drilling and completion stages of operation and serves as an essential barrier against blowouts, that is, the uncontrolled release of crude oil and/or natural gas from a well.

FTA for the BOP system is shown in Figure 12, which was done based on the real data set downloaded from the RAPID-S53 website (https://www.rapid4s53.com). This data set is available in Table 11. Analogously to Section VI-A, the failure modes are represented by two numbers, in the order that they appear from left to right in the graphical representation (again, the first number refers to the system, and the second one stands for the sub-system). It is worth mentioning that these failures occur due to a competing risks mechanism (in which we assume that each of them acts independently), and the safety equipment in question (BOP) is considered to be a repairable system.

First, we can evaluate the proportion of the PLP for each failure cause by using the Duane plot. As it can be observed from Figure 13, the values of the sub-systems are, in general, close to the line, which means that this data set comes from a PLP and our methods can be suitably used.

Table 12 shows the CML estimates and CI 95% for the model parameters. The results presented in this table suggest that the reliability of all components improves over time since the $\hat{\beta}_{jk}$s are less than one. Therefore, we can say that the cause-specific intensity functions of all components decrease over time.

Table 13 displays the estimated intensity functions for each sub-system and the estimated hazard function over some fixed failure times. Observe that the results shown in this table are in agreement with the ones presented in Table 12, that is, the intensity functions decrease over time. We also see that the overall hazard function decreases over time, which may be due to the repair and maintenance effects.

The results presented in Table 12 would also allow us to estimate the reliability function of each system or sub-system, and the reliability function of the overall system. The estimated reliability functions can be obtained from (8),

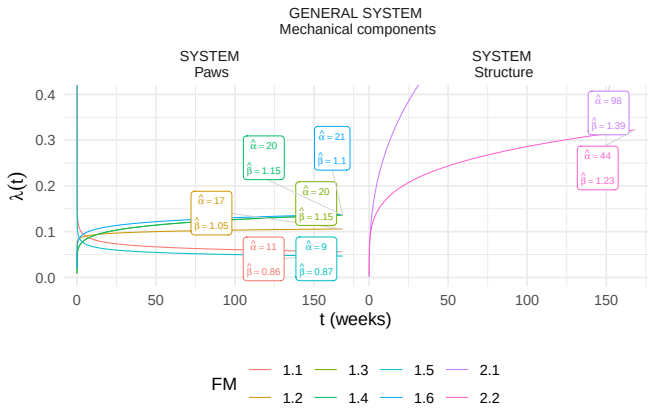

(a) Estimated intensity curves of failure modes.

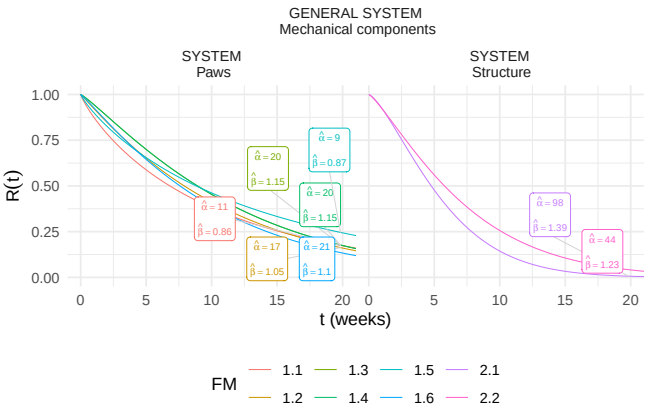

(b) Estimated reliability curves of failure modes.

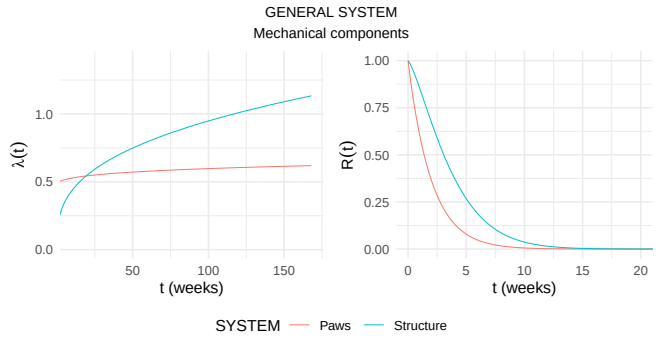

(c) Estimated intensity and reliability curves of systems.

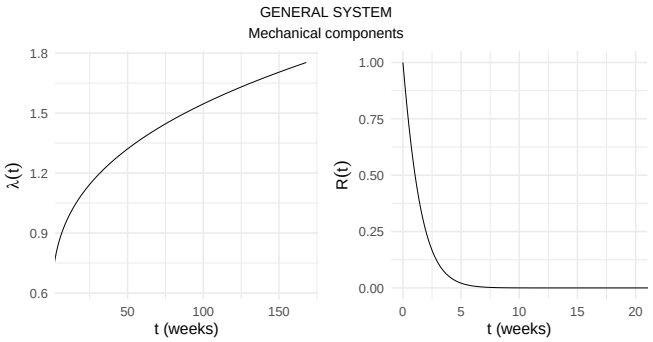

(d) Estimated intensity and reliability curves of general system.

FIGURE 11: General graphical results.

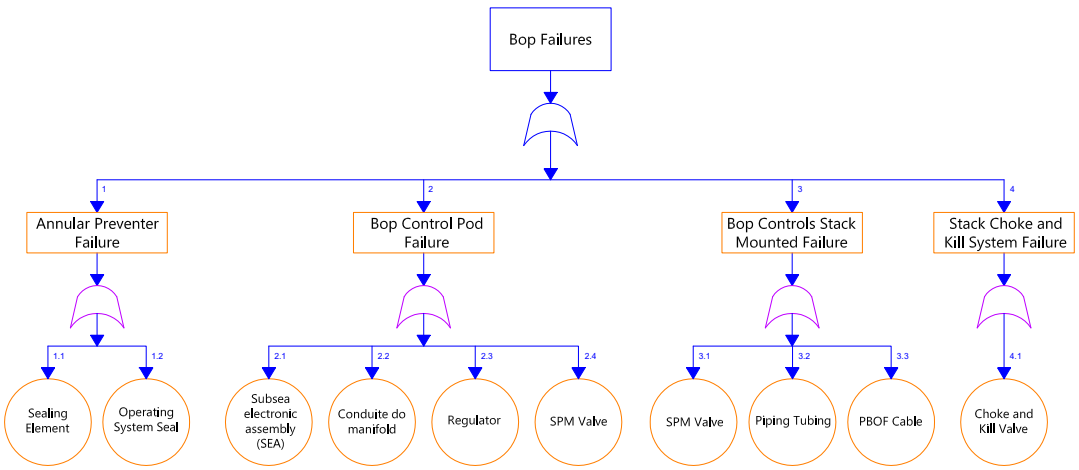

FIGURE 12: FTA of BOP failure.

while the overall reliability function can be obtained from (7), with the parameters substituted by their estimates. Table 14 shows the estimated reliability functions for each sub-system and the estimated overall reliability function over some fixed failure times (which are the same times considered in Table 13). Observe that the overall reliability function, as well as the sub-systems' reliability functions, decrease over time, although at different rates.

TABLE 11: Failure data for a BOP system.

Failure Time	Failure Mode	Failure Time	Failure Mode
52	1.1	8,500	2.4
92	1.1	6	3.1
5,000	1.1	504	3.1
4,320	1.2	720	3.1
6,566	1.2	1,800	3.1
12	2.1	48	3.2
100	2.1	1,450	3.2
50	2.2	2,160	3.2
4,320	2.2	14,780	3.2
720	2.3	200,000	3.2
768	2.3	240	3.3
3,000	2.3	5,640	3.3
8,200	2.3	5,300	4.1
7,776	2.4	6,192	4.1
8,200	2.4		

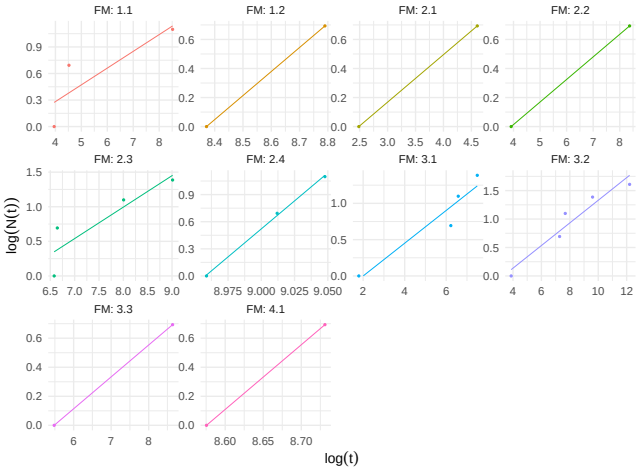

FIGURE 13: Duane plots for the failure modes of a BOP system.

VII. CONCLUDING REMARKS AND FURTHER RESEARCH

In this paper, we introduced a new statistical model for repairable systems subject to hierarchical competing risks under the assumption that the failure modes act independently. The competing risks approach may be useful in the engineering area, since it may lead to a better comprehension of the several failure modes of a system. Therefore, design strategies improve overall system reliability. The hierarchical structure may also be advantageous because sometimes it may record information about which sub-system of a specific system has resulted in the total system failure.

We assumed that the repairs are minimal, and the failure intensity follows a PLP model after a convenient reparametrization. Under a classical framework, we proposed estimators and confidence intervals for the model parameters, whose performances were investigated using a simulation study. In short, the simulation results revealed that the bias-corrected MLEs (or CMLEs) provide better estimates,

TABLE 12: CML estimates and CI 95% of parameters β_{jk} and α_{jk}, considering the BOP failure data.

Parameter	Estimate	CI 95%
β_{11}	0.102	[0.032 ; 0.368]
β_{12}	0.138	[0.033 ; 0.768]
β_{21}	0.058	[0.014 ; 0.322]
β_{22}	0.082	[0.020 ; 0.459]
β_{23}	0.161	[0.059 ; 0.472]
β_{24}	0.208	[0.064 ; 0.753]
β_{31}	0.112	[0.041 ; 0.328]
β_{32}	0.196	[0.080 ; 0.502]
β_{33}	0.097	[0.024 ; 0.541]
β_{41}	0.141	[0.034 ; 0.784]
α_{11}	3.000	[1.090 ; 8.767]
α_{12}	2.000	[0.619 ; 7.225]
α_{21}	2.000	[0.619 ; 7.225]
α_{22}	2.000	[0.619 ; 7.225]
α_{23}	4.000	[1.623 ; 10.242]
α_{24}	3.000	[1.090 ; 8.767]
α_{31}	4.000	[1.623 ; 10.242]
α_{32}	5.000	[2.202 ; 11.668]
α_{33}	2.000	[0.619 ; 7.225]
α_{41}	2.000	[0.619 ; 7.225]

TABLE 13: Estimates of the subsystem-specific and overall intensity functions at different times, considering the BOP failure data.

Intensity	Time (hours)				
	4	24	72	1000	9000
λ_{11}	0.0254	0.0051	0.0019	0.0002	0.0000
λ_{12}	0.0155	0.0033	0.0013	0.0001	0.0000
λ_{21}	0.0155	0.0029	0.0010	0.0001	0.0000
λ_{22}	0.0169	0.0033	0.0012	0.0001	0.0000
λ_{23}	0.0281	0.0063	0.0025	0.0003	0.0000
λ_{24}	0.0164	0.0040	0.0017	0.0002	0.0000
λ_{31}	0.0333	0.0068	0.0026	0.0002	0.0000
λ_{32}	0.0294	0.0070	0.0029	0.0003	0.0001
λ_{33}	0.0170	0.0034	0.0012	0.0001	0.0000
λ_{41}	0.0153	0.0033	0.0013	0.0001	0.0000
λ	0.2128	0.0451	0.0175	0.0018	0.0003

TABLE 14: Estimates of the subsystem-specific and overall reliability functions at different times, considering the BOP failure data.

Reliability	Time (hours)				
	4	24	72	1000	9000
R_{11}	0.3693	0.3025	0.2626	0.1740	0.1122
R_{12}	0.6378	0.5622	0.5117	0.3817	0.2714
R_{21}	0.3427	0.3049	0.2821	0.2292	0.1878
R_{22}	0.4406	0.3867	0.3534	0.2747	0.2125
R_{23}	0.4979	0.3940	0.3289	0.1826	0.0885
R_{24}	0.7299	0.6330	0.5627	0.3698	0.2076
R_{31}	0.3049	0.2340	0.1934	0.1100	0.0593
R_{32}	0.5494	0.4269	0.3479	0.1705	0.0658
R_{33}	0.4970	0.4352	0.3962	0.3026	0.2277
R_{41}	0.6465	0.5704	0.5193	0.3872	0.2745
R	0.0007	0.0001	0.0000	0.0000	0.0000

mainly for the β_{jk} parameters, than the MLEs. Besides, the exact confidence intervals for the α_{jk} parameters give coverage probabilities closer to the nominal value (0.95) than the asymptotic confidence intervals. Finally, the proposed methodology is illustrated through a toy example on a butterfly valve system, an example of a real early-stage project related to an in-pipe robot traction system, and also a real example on a BOP system.

As future works, we intend to derive Bayesian estimators for the model parameters, generalize our results to more than two hierarchical levels, model the dependence among the failure modes (and sub-causes) via shared frailty models, and assume that repairs are either perfect (renewal process model) or imperfect.

REFERENCES

[1] T. Jiang and Y. Liu, "Parameter inference for non-repairable multi-state system reliability models by multi-level observation sequences," Reliability Engineering & System Safety, vol. 166, pp. 3–15, 2017.

[2] Y. Lieping and Q. Zhe, "Failure mechanism and its control of building structures under earthquakes based on structural system concept," Journal of Earthquake and Tsunami, vol. 3, no. 4, pp. 249–259, 2009.

[3] J. Liu, B. Song, and Y. Zhang, "Competing failure model for mechanical system with multiple functional failures," Advances in Mechanical Engineering, vol. 10, no. 5, pp. 1–16, 2018.

[4] M. J. Crowder, Classical competing risks. CRC Press, 2001.

[5] M. Pintilie, Competing risks: a practical perspective. John Wiley & Sons, 2006, vol. 58.

[6] H. Langseth and B. H. Lindqvist, "Competing risks for repairable systems: a data study," Journal of Statistical Planning and Inference, vol. 136, no. 5, pp. 1687–1700, 2006.

[7] S. Tuli, J. Drake, J. Lawless, M. Wigg, and M. Lamberti-Pasculli, "Risk factors for repeated cerebrospinal shunt failures pediatric patients with hydrocephalus," Journal of Neurosurgery, vol. 92, no. 1, pp. 31–38, 2000.

[8] L. H. Crow, "Reliability analysis for complex, repairable systems," Reliability and Biometry, vol. 13, no. 6, pp. 379–410, 1974.

[9] S. E. Rigdon and A. P. Basu, "The power law process: A model for the reliability of repairable systems," Journal of Quality Technology, vol. 21, no. 4, pp. 251–260, 1989.

[10] R. C. P. Reis, E. A. Colosimo, and G. L. Gilardoni, "Hierarchical modelling of power law processes for the analysis of repairable systems with different truncation times: An empirical bayes approach," Brazilian Journal of Probability and Statistics, vol. 33, no. 2, pp. 374–396, 2019.

[11] J. Kyparisis and N. D. Singpurwalla, "Bayesian inference for the weibull process with applications to assessing software reliability growth and predicting software failures," in Com- puter Science and Statistics: Proceedings of the Sixteenth Symposium on the Interface (ed. L. Billard). Elsevier Science Publishers B. V. (North Holland), Amsterdam, 1985, pp. 57–64.

[12] L. H. Crow, "Confidence interval procedures for the weibull process with applications to reliability growth," Technometrics, vol. 24, no. 1, pp. 67–72, 1982.

[13] H. Ascher and H. Feingold, "Repairable systems reliability: Modelling, inference, misconceptions and their causes," Lecture Notes in Statistics, vol. 7, 1984.

[14] M. Engelhardt and L. J. Bain, "On the mean time between failures for repairable systems," IEEE Transactions on Reliability, vol. 35, no. 4, pp. 419–422, 1986.

[15] J. T. Duane, "Learning curve approach to reliability monitoring," IEEE Transactions on Aerospace, vol. 2, no. 2, pp. 563–566, 1964.

[16] B. Klefsjo and U. Kumar, "Goodness-of-fit tests for the power-law process based on the ttt-plot," IEEE Transactions on Reliability, vol. 41, no. 4, pp. 593–598, 1992.

[17] R. D. Baker, "Some new tests of the power law process," Technometrics, vol. 38, no. 3, pp. 256–265, 1996.

[18] M. Bhattacharjee, J. V. Deshpande, and U. V. Naik-Nimbalkar, "Unconditional tests of goodness of fit for the intensity of time-truncated nonhomogeneous poisson processes," Technometrics, vol. 46, no. 3, pp. 330–338, 2004.

[19] S. E. Rigdon and A. P. Basu, Statistical methods for the reliability of repairable systems. Wiley New York, 2000.

[20] S. K. Bar-Lev, I. Lavi, and B. Reiser, "Bayesian inference for the power law process," Annals of the Institute of Statistical Mathematics, vol. 44, no. 4, pp. 623–639, 1992.

[21] M. Guida, R. Calabria, and G. Pulcini, "Bayes inference for a non-homogeneous poisson process with power intensity law (reliability)," IEEE Transactions on Reliability, vol. 38, no. 5, pp. 603–609, 1989.

[22] M. D. de Oliveira, E. A. Colosimo, and G. L. Gilardoni, "Bayesian inference for power law processes with applications in repairable systems," Journal of Statistical Planning and Inference, vol. 142, no. 5, pp. 1151–1160, 2012.

[23] A. Somboonsavatdee and A. Sen, "Statistical inference for power-law process with competing risks," Technometrics, vol. 57, no. 1, pp. 112–122, 2015.

[24] H. Wang and H. Pham, Reliability and Optimal Maintenance. Springer London, 2006.

[25] T. Aven, "Optimal replacement under a minimal repair strategy, a general failure model," Advances in Applied Probability, vol. 15, no. 01, pp. 198–211, 1983.

[26] R. Barlow and L. Hunter, "Optimum preventive maintenance policies," Operations research, vol. 8, no. 1, pp. 90–100, 1960.

[27] T. Aven and U. Jensen, "A general minimal repair model," journal of applied probability, vol. 37, no. 01, pp. 187–197, 2000.

[28] M. Finkelstein, "Minimal repair in heterogeneous populations," Journal of Applied Probability, vol. 41, no. 01, pp. 281–286, 2004.

[29] T. A. Mazzuchi and R. Soyer, "A bayesian perspective on some replacement strategies," Reliability Engineering & System Safety, vol. 51, no. 3, pp. 295–303, 1996.

[30] L. Doyen and O. Gaudoin, "Classes of imperfect repair models based on reduction of failure intensity or virtual age," Reliability Engineering & System Safety, vol. 84, no. 1, pp. 45–56, 2004.

[31] L. Bain, Statistical analysis of reliability and life-testing models: theory and methods. Routledge, 2017.

[32] O. Gaudoin, B. Yang, and M. Xie, "Confidence intervals for the scale parameter of the power-law process," Communications in Statistics-Theory and Methods, vol. 35, no. 8, pp. 1525–1538, 2006.

[33] B. X. Wang, M. Xie, and J. X. Zhou, "Generalized confidence interval for the scale parameter of the power-law process," Communications in Statistics-Theory and Methods, vol. 42, no. 5, pp. 898–906, 2013.

[34] D. R. Cox and N. Reid, "Parameter orthogonality and approximate conditional inference," Journal of the Royal Statistical Society. Series B (Methodological), pp. 1–39, 1987.

[35] M. A. Bin Yusof and N. H. B. Abdullah, "Failure mode and effect analysis (fmea) of butterfly valve in oil and gas industry," JOURNAL OF ENGINEERING SCIENCE AND TECHNOLOGY, vol. 11, pp. 9–19, 2016.

[36] A. Høyland and M. Rausand, System reliability theory: models and statistical methods. John Wiley & Sons, 2009, vol. 420.

[37] S. Wu and P. Scarf, "Two new stochastic models of the failure process of a series system," European Journal of Operational Research, vol. 257, no. 3, pp. 763–772, 2017.

[38] W. Q. Meeker and L. A. Escobar, Statistical Methods for Reliability Data, ser. Wiley Series in Probability and Statistics. Wiley, 2014. [Online]. Available: https://books.google.com.br/books?id=Q01YBAAAQBAJ

[39] D. R. Cox and E. J. Snell, "A general definition of residuals," Journal of the Royal Statistical Society. Series B (Methodological), pp. 248–275, 1968.

[40] G. M. Cordeiro and R. Klein, "Bias correction in arma models," Statistics & Probability Letters, vol. 19, no. 3, pp. 169–176, 1994.

[41] D. Firth, "Bias reduction of maximum likelihood estimates," Biometrika, vol. 80, no. 1, pp. 27–38, 1993.

[42] H. Jeffreys, "An invariant form for the prior probability in estimation problems," in Proceedings of the Royal Society of London A: Mathematical, Physical and Engineering Sciences, vol. 186, no. 1007. The Royal Society, 1946, pp. 453–461.

[43] T. Kimura, T. Tanaka, K. Fujimoto, and K. Ogawa, "Hydrodynamic characteristics of a butterfly valveâĂŤprediction of pressure loss characteristics," ISA transactions, vol. 34, no. 4, pp. 319–326, 1995.

[44] S. Corbera, J. L. Olazagoitia, and J. A. Lozano, "Multi-objective global optimization of a butterfly valve using genetic algorithms," ISA transactions, vol. 63, pp. 401–412, 2016.

[45] M. A. B. Yusof and N. H. B. Abdullah, "Failure mode and effect analysis (fmea) of butterfly valve in oil and gas industry."

[46] X. G. Song, L. Wang, S. H. Baek, and Y. C. Park, "Multidisciplinary optimization of a butterfly valve," ISA transactions, vol. 48, no. 3, pp. 370–377, 2009.
[47] S. Suresh, Fatigue of materials. Cambridge university press, 1998.
[48] S. Hasunuma, S. Oki, K. Motomatsu, and T. Ogawa, "Fatigue life prediction of carbon steel with machined surface layer under low-cycle fatigue," International Journal of Fatigue, vol. 123, pp. 255–267, 2019.
[49] E. Drægebø, "Reliability analysis of blowout preventer systems - a comparative study of electro-hydraulic vs. all-electric bop technology," Master's thesis, Norwegian University of Science and Technology, Norway, 2014.